

# Rough parameter dependence in climate models and the role of Ruelle-Pollicott resonances

Mickaël David Chekroun, J. David Neelin, Dmitri Kondrashov, James C. McWilliams<sup>1</sup>, and Michael Ghil

Department of Atmospheric and Oceanic Sciences and Institute of Geophysics and Planetary Physics, University of California, Los Angeles, CA 90095

Contributed by James C. McWilliams, November 22, 2013 (sent for review August 9, 2013)

Despite the importance of uncertainties encountered in climate model simulations, the fundamental mechanisms at the origin of sensitive behavior of long-term model statistics remain unclear. Variability of turbulent flows in the atmosphere and oceans exhibits recurrent large-scale patterns. These patterns, while evolving irregularly in time, manifest characteristic frequencies across a large range of time scales, from intraseasonal through interdecadal. Based on modern spectral theory of chaotic and dissipative dynamical systems, the associated low-frequency variability may be formulated in terms of Ruelle-Pollicott (RP) resonances. RP resonances encode information on the nonlinear dynamics of the system, and an approach for estimating them—as filtered through an observable of the system—is proposed. This approach relies on an appropriate Markov representation of the dynamics associated with a given observable. It is shown that, within this representation, the spectral gap—defined as the distance between the subdominant RP resonance and the unit circle—plays a major role in the roughness of parameter dependences. The model statistics are the most sensitive for the smallest spectral gaps; such small gaps turn out to correspond to regimes where the low-frequency variability is more pronounced, whereas autocorrelations decay more slowly. The present approach is applied to analyze the rough parameter dependence encountered in key statistics of an El-Niño–Southern Oscillation model of intermediate complexity. Theoretical arguments, however, strongly suggest that such links between model sensitivity and the decay of correlation properties are not limited to this particular model and could hold much more generally.

climate dynamics | Markov operators | parametric dependence | sensitivity bounds | uncertainty quantification

Sensitive behavior of long-term general circulation model (GCM) statistics is attracting increased attention (1–3), but its origin and fundamental mechanisms remain unclear. These sensitive-behavior issues are of practical, as well as theoretical, importance in climate dynamics and elsewhere (4). For some GCMs, involving millions of variables, circumstances have been found where certain climate observables vary smoothly through a plausible parameter range (5) or where linear response theory applies over some range (6). On the other hand, this may not hold for every observable or parameter, and concerns arise regarding the role of some type of “structural instability” in sensitive parameter dependence (1, 2, 4).

The low-order Lorenz (L63) model (7) illustrates some of the relevant issues. Various statistics exhibit linear dependence over a broad range of parameters for which the dynamics is chaotic (e.g., figure 2 of ref. 8). The statistics’ linear dependence coexists here with structural instability of this model’s global attractor, as small variations in the parameters cause a plethora of topological changes (9). In particular, the unstable periodic orbits that appear or disappear as a parameter changes may only have a negligible effect on the model’s physical invariant measure (see below), if their period is longer than the decorrelation time of the dynamics.

In general, the role played by a system’s mixing and harmonic properties on the nature of its response has been only partially addressed. Only very specific results exist, in the deterministic setting, to support the idea that linear response of the long-term

statistics (and of local variations of physical measures) may still hold in the absence of (topological) structural stability (10). For stochastic systems, more general results have been obtained (11), but it is still a challenge to relate the size of the parameter interval over which linear response may hold to the system’s mixing properties. Conditions for smooth but nonlinear response (e.g., quadratic) or else for rough parameter dependence—with many highly local variations in response over a given parameter interval—to occur are also poorly known.

To help us understand the circumstances in which one may expect one type of behavior rather than the other, we cast here this problem in a theoretical framework based on the modern spectral theory of dynamical systems (10, 12–19). The approach is illustrated on an El Niño–Southern Oscillation (ENSO) model of intermediate complexity. The model is governed by a system of coupled partial differential equations (PDEs), and it exhibits different degrees of roughness in its parameter dependence in different regimes. The relationship of statistics such as the power spectrum to dynamical features known as Ruelle-Pollicott (RP) resonances (20–22) is outlined below and suggests the usefulness of estimating these resonances—despite the challenge of doing so in high-dimensional systems. To do so, we introduce here a unique approach that estimates these resonances as filtered through an observable chosen from the simulated scalar time series. This approach allows us to shed light on subtle relationships between the nonlinear mixing rate in the system’s phase flow and the nature of the parameter dependence of its long-term statistics.

## Intermediate ENSO Model and Its Key Properties

The intermediate-complexity ENSO model examined in this study is the Jin-Neelin (JN) model (23) forced by the seasonal cycle. The way we include the latter differs from the one used

### Significance

It is shown on a geophysical fluid model that the sensitive dependence on parametric variations of a given set of observations is related to the dominant modes of variability of the flow, as encoded through the Ruelle-Pollicott resonances. The latter are estimated by Markov modeling techniques. Such modeling and analysis methods can be used for any type of high-dimensional dissipative and chaotic dynamical systems.

Preliminary versions of this work were presented by M.D.C. and J.D.N. at the workshop on Stochastic Modeling of the Oceans and the Atmosphere, at the Institute of Mathematics and its Applications, March 11–15, 2013, University of Minnesota, Minneapolis; at the workshop on Stochastics in Geophysical Fluid Dynamics, at the American Institute of Mathematics, February 4–8, 2013, Palo Alto, CA; and at the AMS Special Session on Environmental Mathematics: Evaluate the Past Climate Changes and Model the Future Climate Variations, at the Joint Mathematics Meetings in San Diego, CA, January 10–12, 2013, San Diego.

Author contributions: M.D.C., J.D.N., J.C.M., and M.G. designed research; M.D.C. and D.K. performed research; M.D.C. contributed new reagents/analytic tools; M.D.C. and D.K. analyzed data; and M.D.C., J.D.N., J.C.M., and M.G. wrote the paper.

The authors declare no conflict of interest.

Freely available online through the PNAS open access option.

<sup>1</sup>To whom correspondence should be addressed. E-mail: jcm@atmos.ucla.edu.

This article contains supporting information online at [www.pnas.org/lookup/suppl/doi:10.1073/pnas.1321816111/-DCSupplemental](http://www.pnas.org/lookup/suppl/doi:10.1073/pnas.1321816111/-DCSupplemental).



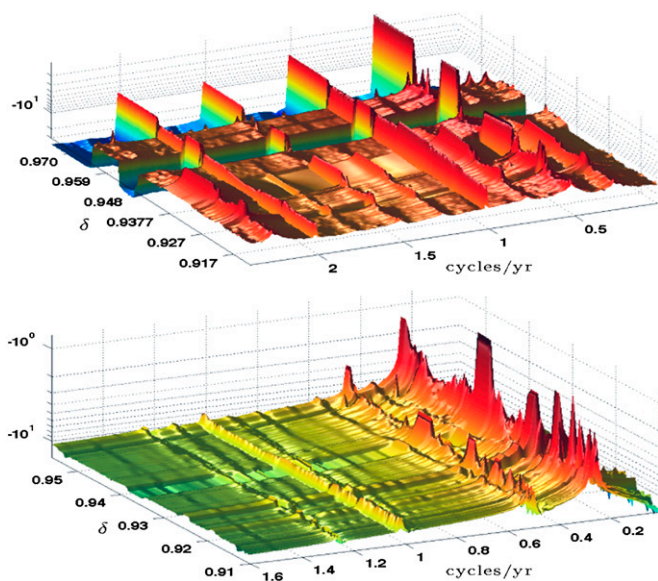


**Fig. 2.**  $\delta$ -Parameter dependence of the power spectrum of the Niño-3 SSTs for the rapidly mixing regime (Upper;  $\delta_s=0.95$ ) and the slowly mixing one (Lower;  $\delta_s=0.1$ ). For presentation purposes, the interval  $0.957 \leq \delta \leq 0.965$ , where the dynamics is periodic, is removed from the lower panel, whereas it is included for the rapidly mixing regime, where it corresponds to chaotic dynamics.

understand and quantify the occurrence of rough parameter dependence in complex systems, as illustrated in the previous section.

To simplify the presentation, let  $X = \mathbb{R}^d$  be a Euclidean vector space of dimension  $d$ , subject to a one-parameter group of smooth transformations  $\{S_t\}_{t \in \mathbb{R}}$ , associated with the flow of a smooth but nonlinear system of ordinary differential equations, given by  $\dot{x} = \mathbf{F}(x)$ . The main objective of the spectral theory of chaotic DDSs is to study the evolution of probability laws induced by  $S_t$  instead of studying individual trajectories that exhibit chaotic behavior.

This objective is achieved by examining the family of Perron-Frobenius operators. Such a family  $\{\mathcal{L}_t\}$ , also known as transfer operators (12, 15, 17, 18, 26, 27), acts on probability measures  $\nu$  and it is given by

$$\mathcal{L}_t \nu(E) := \nu(S_t^{-1}(E)), \quad [1]$$

for any measurable set  $E \subset X$ . It gives the measure with respect to  $\nu$  of the ensemble of points in  $X$  that occupy  $E$  at time  $t$ . Note that sometimes  $\mathcal{L}_t \nu$  is denoted by  $(S_t)_* \nu$ , i.e., the pushforward of the measure  $\nu$  by  $S_t$ .

Under mild assumptions on  $\mathbf{F}$  and  $\nu$ , it can be shown that  $\mathcal{L}_t \nu$  is in fact a weak solution  $\eta$  emanating from  $\nu$  at  $t = 0$ , in the Schwartz sense of distributions, of the transport equation

$$\partial_t \eta + \text{div}(\eta \mathbf{F}) = 0, \quad [2]$$

on  $[0, \infty) \times X$ , where the operator  $\text{div}$  is the divergence operator on  $X$ . In parallel, the study of the evolution of densities associated with  $\nu$  with due attention to the proper functional spaces in which these densities live (10, 12–19), is of prime importance for the theory.

It can be proven for hyperbolic dynamical systems and it is observed experimentally for many others (15, 30, 31) that a common feature of DDSs is the transformation of the initial Lebesgue measure  $m_0$  into a measure  $\mathcal{L}_t m_0$  that has still a finite density with respect to  $m_0$  but that exhibits finer and finer structure, as time  $t$  evolves. Asymptotically, an invariant measure  $\mu$  of Sinai-Ruelle-Bowen (SRB) type is generally reached (15, 30) as  $t \rightarrow +\infty$ . This measure is physical in the sense that  $\langle f \rangle_\mu := \int_X f d\mu = \lim_{L \rightarrow \infty} \frac{1}{L} \int_0^L f(S_t x) dt$  for  $m_0$ , almost all  $x \in X$ , and

any sufficiently smooth observable  $f : X \rightarrow \mathbb{R}$ . This property is often referred to as the chaotic hypothesis that, roughly speaking, expresses an extension of the ergodic hypothesis to non-Hamiltonian systems (31).

Such a measure  $\mu$  is typically singular with respect to  $m_0$  while exhibiting smooth density in the expanding directions, or unstable manifolds, whose Hausdorff dimension is strictly less than  $d$ . In other words, the initial measure  $m_0$  flows into microscopic scales of vanishing volume, whereas on the macroscopic scale,  $\mu$ , supported by the unstable manifolds, is the only information from  $m_0$  that remains visible after the dynamics acted over an infinite amount of time.

For Anosov flows (14), one considers functional spaces  $\mathfrak{B}$  that capture such stretching and contracting effects of the dynamics and can then prove that the SRB measure  $\mu$  may be equivalently characterized as the stationary solution of Eq. 2. In ref. 14, it is then shown that the related statistical properties of the flow are accurately described by the spectral properties of the transfer operators acting on  $\mathfrak{B}$ . Moreover,  $\{\mathcal{L}_t\}_{t \geq 0}$  is a strongly continuous semigroup in  $\mathfrak{B}$ , uniformly bounded in  $t$ , and its generator is given by  $\mathcal{A} \cdot = -\text{div}(\mathbf{F} \cdot)$ , where  $\mathbf{F}$  is the vector field generating the Anosov flow. As a consequence, the spectrum of  $\mathcal{A}$  is contained in the left-half complex plane,  $\{z \in \mathbb{C} : \text{Re}(z) \leq 0\}$ , and its resolvent  $R(z) = (z\text{Id} - \mathcal{A})^{-1}$ —which determines the spectral properties of  $\mathcal{A}$ —is a well-defined bounded operator on  $\mathfrak{B}$  that admits, for all  $f \in \mathfrak{B}$  and  $z \in \mathbb{C}$  with  $\text{Re}(z) > 0$ , the following integral representation:

$$R(z)f = \int_0^\infty e^{-zt} \mathcal{L}_t f dt. \quad [3]$$

It can then be proven that the spectrum of the generator  $\mathcal{A}$  on  $\mathfrak{B}$  consists only of isolated eigenvalues of finite multiplicity within a strip  $-\gamma < \text{Re}(z) \leq 0$ , for some  $\gamma > 0$  that depends on the stretching and contracting rate of the dynamics (14); the rest of the spectrum is continuous and located in  $\{z \in \mathbb{C} : \text{Re}(z) \leq -\gamma\}$ . In addition, the eigenspace associated with the null eigenvalue is spanned by the set of SRB measures; this set is reduced to only one such measure provided the zero is simple. We assume henceforth that the latter is the case, and  $\mu$  will always refer to this unique SRB measure.

The extension of such rigorous results to other classes of chaotic DDSs is still a major challenge. However, a widespread conjecture is that the global picture is relevant to most chaotic DDSs. In other words, the spectrum  $\sigma(\mathcal{A})$  of  $\mathcal{A} = -\text{div}(\mathbf{F} \cdot)$  on some appropriate functional spaces  $\mathfrak{B}$  for such a system consists always of the disjoint union of a continuous part and a discrete part. These two are called, respectively, the essential spectrum  $\sigma_{\text{ess}}(\mathcal{A})$ , and the point spectrum  $\sigma_p(\mathcal{A})$  (13). When the existence of a (unique) SRB measure  $\mu$  is assumed, classical function spaces, such as  $L^1_\mu(X)$  or  $L^2_\mu(X)$ , are suitable (17, 18).

In the interesting cases, i.e., when the point spectrum is not trivially reduced to  $\{0\}$ , it is typically located in a vertical strip of the complex plane whose points are known as the RP resonances (20–22). These resonances give precise information on correlation decay and on the power spectrum. We describe this information via formal mathematical arguments, referring to the specialized literature for their rigorous treatment.

Note first that, by making the change of variables  $y = S_t(x)$

$$\int \mathcal{L}_t f \cdot g d\mu = \int f \cdot g \circ S_t d\mu, \quad [4]$$

where  $f \cdot g$  denotes the product map  $x \mapsto f(x)g(x)$ . This equation results from the general change-of-variables formula  $\int g d((S_t)_* \nu) = \int g \circ S_t d\nu$ , with  $d\nu = f d\mu$  (32). Here the action  $\mathcal{L}_t f$  of  $\mathcal{L}_t$  on the density  $f$  with respect to  $\mu$  is defined by  $\mathcal{L}_t f := d((S_t)_* \nu) / d\mu$ , the Radon-Nykodim derivative of  $\mathcal{L}_t \nu$  with respect to  $\mu$  (17, 18) (see also *SI Text*).

If we assume, without loss of generality, that  $f$  and  $g$  have a vanishing  $\mu$ -ensemble mean, i.e.,  $\langle f \rangle_\mu = \langle g \rangle_\mu = 0$ , then the right side of Eq. 4 denotes the correlation function  $\rho_{f,g}(t) = \int f \cdot g \circ S_t \, d\mu$ . From the physical property of the SRB measure  $\mu$ , this function equals for almost all  $x \in X$ , the more familiar cross-correlation coefficient at lag  $t$ , given by  $C_{f,g}(t) = \lim_{L \rightarrow \infty} \frac{1}{L} \int_0^L f(S_s(x))g(S_{t+s}(x))ds$ .

Using Eq. 3, one can rewrite the Fourier transform of  $\rho_{f,g}(t)$ , given by  $\hat{\rho}_{f,g}(\omega) := \int_0^\infty \rho_{f,g}(t)e^{-i\omega t} dt$ , as

$$\hat{\rho}_{f,g}(\omega) = \int_0^\infty e^{-i\omega t} \left( \int \mathcal{L}_t f \cdot g \, d\mu \right) dt = \int \left( \int_0^\infty e^{-i\omega t} \mathcal{L}_t f \, dt \right) g \, d\mu \tag{5}$$

$$= \int g R(i\omega) f \, d\mu.$$

The meromorphic extension into the complex plane of  $\hat{\rho}_{f,g}(\omega)$ , via Eq. 5, tells us that the poles of the resolvent  $R(i\omega)$ —which correspond to the RP resonances—introduce singularities into the complex Fourier transform, where  $\omega \in \mathbb{C}$  is a complex frequency. These poles will manifest themselves in the power spectrum as peaks that stand out over a continuous background at frequency  $\xi$ , if the corresponding RP resonances with imaginary part  $\xi$  are close enough to the imaginary axis. The continuous background has its origin in the continuous part of  $\sigma(\mathcal{A})$ .

Note that the position of the poles depends only on the system considered, whereas their residues depend on the observable monitored (21). As a result, some peaks in the power spectrum may disappear from observable to observable, depending on how large or small their residues may be. Ruelle (21, 22) and Pollicott (20) introduced this description of RP resonances as poles in the meromorphic extension of  $\hat{\rho}_{f,g}(\omega)$  that are responsible for bumps in the power spectrum; they also connected these resonances to the decay rate of correlations.

The latter connections, between RP resonances and correlation decay, are subtler and closely related to the model flow's relaxation toward the SRB measure  $\mu$  as  $t \rightarrow +\infty$ . If 0 is the only eigenvalue of  $\mathcal{A}$  on the imaginary axis, the system is mixing, and the existence of a gap between 0 and the rest of the spectrum  $\sigma(\mathcal{A})$  governs the rate of convergence of  $\mathcal{L}_t \mu$  toward  $\mu$ . The size  $\tau$  of this gap is given by  $\tau = \min\{|\operatorname{Re}(\lambda)|, \lambda \in \sigma(\mathcal{A}) \setminus \{0\}\} > 0$ .

More precisely, in such a case, one can prove that, for any probability measure  $\nu$  that has density  $\psi$  with respect to the Lebesgue measure and for all suitably chosen test functions  $\varphi$

$$\int \varphi \, d(\mathcal{L}_t \nu) = \int \varphi \, d\mu + \mathcal{O}(e^{-t/\tau}). \tag{6}$$

The main step in establishing Eq. 6 is to prove the existence of the spectral gap  $\tau > 0$ ; remaining steps rely on the inversion of Eq. 3 and the properties of the resolvent  $R(z)$  (20). Furthermore, because  $\int \varphi \, d(\mathcal{L}_t \nu) = \int \psi \cdot \varphi \circ S_t \, d\mu_0$  and  $\langle \psi \rangle_{\mu_0} = 1$ , one obtains from Eq. 6 that  $|\int \psi \cdot \varphi \circ S_t \, d\mu_0 - \langle \varphi \rangle_\mu| \rightarrow 0$  at the exponential rate  $\tau$ . Thus, the spectral gap  $\tau$  controls the decay of correlations, when the system is initiated out of the SRB equilibrium  $\mu$ .

These arguments can be made rigorous in the context of Anosov flows (19), but, in general, the decay of correlations can be subexponential. This situation arises when the RP resonances are arbitrarily close to the imaginary axis. If  $\tau > 0$ , and the discrete spectrum is nontrivial, RP resonances lead to modulations in the decay of correlations, which correspond to peaks in the power spectrum.

Thus, RP resonances provide powerful theoretical tools to describe the variability in time of the system's flow, in terms of spectral properties of the operator  $\mathcal{A} = -\operatorname{div}(\mathbf{F})$ , where  $\mathbf{F}$  is the nonlinear vector field that generates the flow. Key features of this variability include peaks in the power spectrum and the decay rate of correlations.

The original treatment of RP resonances (20, 22) was based, in fact, on a different approach, which used Markov partitions of the dynamics (15). The spectrum  $\sigma(\mathcal{L}_t)$  of  $\mathcal{L}_t$ —which lives within the unit disk—was analyzed, rather than that of  $\mathcal{A}$ , in the left-half plane. However, similar results relating the RP resonances to the decay of correlations and to the power spectrum were established. We preferred to follow here the framework of ref. 14 because of its connections with the fundamental Eq. 2, whose analysis may benefit from PDE techniques (33) and the spectral theory of semigroups and their generators.

The latter theory offers conceptual advantages for describing the relations between the RP resonances and the decay of correlations on one hand and the power spectrum on the other. Nevertheless, for practical purposes, the approximation by a discrete time Markov process from a sequence of observations of the dynamics may be used to provide estimates of the (filtered) RP resonances when for instance the direct computation of  $\sigma(\mathcal{A})$  is out of reach for large systems such as considered in this article. Such an approach is described below.

### Estimating RP Resonances from Observables

In a low-dimensional phase space, Markov partitions provide natural tools to study the spectral properties of  $\mathcal{A}$  or  $\mathcal{L}_t$ , the latter being approximated by a stochastic matrix  $P$  in the case of maps (26, 27). In essence, Ulam-type methods approximate the dynamics in phase space by a Markov chain whose transition probabilities are estimated from many simultaneous iterations of the map of interest over a large ensemble of initial data (26, 27). This approach can be rigorously justified for a large class of expanding or Anosov maps (27), and it can be used in the numerical estimation of RP resonances for low-dimensional models (34), although some drawbacks may arise in applications (35).

In a large-dimensional phase space, such as the one where the fJN model's dynamics takes place, with  $d \simeq 400$ , the Ulam approach becomes computationally intractable. A cheaper and less ambitious approach consists of taking a single observable  $h$  and, instead of trying to approximate the full transfer operator  $\mathcal{L}_t$ , seek a decomposition of the autocorrelation function associated with  $h$  from a long simulation into a sum of complex exponentials. In principle, this gives the positions of the RP resonances corresponding to nonvanishing residues associated with  $h$ . Padé approximation or Prony's method are typically used (36). The main drawback of these techniques lies in the number of exponentials to be fitted to the signal, which may lead to an inaccurate estimation of RP resonance (35).

We propose here an intermediate approach based on sufficiently long model runs that exploit Ulam's ideas but apply them to a Markov operator  $\mathfrak{T}$  (17) that acts on a space of functions that depends only on the observed variables. As we will show, this operator  $\mathfrak{T}$  is rigorously associated with the full transfer operator  $\mathcal{L}$  of the dynamics, given an observable  $h$  and the physical measure  $\mu$  of the underlying map. The operator  $\mathfrak{T}$  can then be approximated by a stochastic matrix  $P$ , which is estimated by computing a classical maximum likelihood estimator (MLE) (37),  $\hat{P}$ , from the sequence of observations  $\{x_n\} := \{h(\mathbf{x}_n) : n = 1, \dots, N\}$ .

When this sequence is long enough, the eigenvalues of  $\hat{P}$  provide crucial information about, and actual estimates of, the dominant RP resonances, as filtered by  $h$ , i.e., the resonances that correspond to nonvanishing residues and yield the largest contributions to the power spectrum of  $h$  (SI Text). Clearly, the more delicate point is the existence of such an operator  $\mathfrak{T}$ , which we show hereafter for a broad class of chaotic systems. Details of a more practical nature about the approximation of  $\mathfrak{T}$  then follow and are applied to the fJN model. Finally, note that our approach is complementary to the one in ref. 38 for Hamiltonian systems; the latter focuses on the related but distinct question of identifying metastable features of the dynamics.

**Markov Operators from Observables of Chaotic Systems.** In this section, we consider discrete dynamical systems given by  $\mathbf{x}_{n+1} = \mathbf{F}(\mathbf{x}_n, \mathbf{u}_n)$ ,

where  $\mathbf{x}_n \in X = \mathbb{R}^d$ , and  $\mathbf{u}_n$  is assumed to be a periodic forcing of period  $m$ . We assume furthermore that  $S_{n,p}$ —the solution operator that evolves the system from its state at time  $p$  to its state at time  $n$ —is well defined for any  $p \leq n$  and that the semigroup property  $S_{n,q} = S_{n,p} \circ S_{p,q}$  holds for all  $q \leq p \leq n$ .

Chaotic behavior is synonymous here to the existence of a unique time-dependent, necessarily  $m$ -periodic SRB measure  $\mu_n$ , which attracts the Lebesgue measure in a pullback sense, i.e.,  $(S_{n,p})_* \rho \rightarrow \mu_n$  as  $p \rightarrow -\infty$ , where  $\rho$  is the Lebesgue measure (39). The latter property is assumed to hold in the absence of chaos as well, e.g., for a global limit cycle or for a quasi-periodic behavior. Note that in the presence of a positive Lyapunov exponent, due to a theorem of Ledrappier and Young, one can ensure the existence of such SRB measures by perturbing the governing evolution equations with an appropriate noise of very small intensity (39).

For simplicity, we denote now by  $S$  the map  $S_{m,0}$  whose iterations give the states of the system at any integer multiple of the period  $m$  of the forcing. This map is called the time- $m$  map. By using an analog of Eq. 1 for discrete time, a transfer operator  $\mathcal{L}$  can be associated to  $S$ . By  $m$ -periodicity and from our assumptions on  $S_{n,p}$ , the dynamical system generated now by  $S$  possesses  $\mu := \mu_m$  as an SRB measure. We consider the system in this statistical equilibrium and define  $\mathcal{L}$  acting on densities  $f$  with respect to  $\mu$  by  $\mathcal{L}f := d\mathcal{L}\nu/d\mu$  for any  $f \in L^1_\mu(X)$  such that  $d\nu = f d\mu$ .

Let  $\mathfrak{A}$  be the (compact) support of  $\mu$  and define the transition probability  $\mathfrak{p}(C, D)$  for the map  $S$  of reaching the Borel set  $D$  of  $\mathfrak{A}$  from the Borel set  $C$  of  $\mathfrak{A}$  by

$$\mathfrak{p}(C, D) := \frac{\mu(C \cap S^{-1}D)}{\mu(C)} = \frac{\langle \chi_C, \chi_D \rangle_{1,\infty}}{\mu(C)}, \quad [7]$$

where  $\chi_A$  is the characteristic function of set  $A$ , and the latter equality results from Eq. 4, where  $\langle f, g \rangle_{1,\infty} := \int f \cdot g d\mu$  for  $f \in L^1_\mu(X)$  and  $g \in L^\infty(X)$ . We now state the main result on which we will rely to explain the puzzling parameter dependence of the fJN model pointed out in Fig. 1 (SI Text).

**Theorem A.** *Let  $h: X \rightarrow \mathbb{R}^p$  be a continuous observable of the dynamical system generated by  $S$ , with  $p < d$ . Assume that  $S$  possesses a unique physical measure  $\mu$  with support  $\mathfrak{A}$ . Let  $\mathcal{V}$  be the set  $h(\mathfrak{A})$  and  $\mathfrak{m} := h_*\mu$  be the pushforward of  $\mu$  by  $h$ . Then there exists a Markov operator  $\mathfrak{T}$  acting on  $L^1_{\mathfrak{m}}(\mathcal{V})$  such that  $\mathfrak{T}\chi_V = \chi_V$  and such that, for any Borel sets  $E$  and  $F$  of  $\mathcal{V}$*

$$\langle \mathfrak{T}\chi_E, \chi_F \rangle_{1,\infty} = \mathfrak{m}(E)\mathfrak{p}(h^{-1}(E), h^{-1}(F)). \quad [8]$$

The proof of this result is a consequence of the general disintegration theorem of measures, from which  $\mathfrak{T}$  can be constructed explicitly (SI Text). From Eq. 7, we see that  $\mathfrak{T}$  determines the transition probabilities for any pair  $(C, D)$  of Borel sets, and conversely, Eq. 8 shows that, when restricting the transition probabilities  $\mathfrak{p}(C, D)$  to pairs of the form  $(h^{-1}(E), h^{-1}(F))$ , the Markov operator  $\mathfrak{T}$  determines these exactly.

In general, the latter pairs run across a coarser family of subsets than the former, being a sub- $\sigma$ -algebra of the Borel sets. We may thus say that  $\mathfrak{T}$  characterizes a coarse-graining—induced by the observable  $h$ —of the actual dynamics, along with its transitions. At the same time, the operator  $\mathfrak{T}$  given by theorem A offers a natural way to represent rigorously the sequence of observations  $\{h(\mathbf{x}_n) : n = 1, \dots, N\}$  as a finite-size sample of the discrete-time Markov process associated with  $\mathfrak{T}$  (SI Text, corollary B). In brief, theorem A provides a rigorous basis for the assertion that the simple fact of observing a deterministic system allows us to represent the unobserved variables as noise (SI Text). The theory of Markov process can thus shed considerable light on the spectral properties of  $\mathcal{L}$  filtered by  $h$ , as we illustrate in the next sections.

**Stochastic Matrices from Observations and RP Resonances.** We assume hereafter that an SRB measure  $\mu$  exists for the time  $m$  map  $S$  associated with the truncated version of the fJN model in  $X = \mathbb{R}^d$  with  $d = 408$ . The goal here is to analyze the spectrum  $\sigma(\mathfrak{T})$  of  $\mathfrak{T}$  in  $L^1_{\mathfrak{m}}(\mathcal{V})$  and, more specifically, its dominant contributions. To approximate the dominant part of  $\sigma(\mathfrak{T})$ , we use a Galerkin procedure on a uniform grid of the one-dimensional set  $\mathcal{V} = h(\mathfrak{A}) := \bigcup_{k=1}^M J_k$ .

The eigenvalue problem  $\mathfrak{T}\psi = \lambda\psi$  is projected onto the problem  $\mathfrak{T}_M \mathbf{v} = \lambda \mathbf{v}$  in the subspace spanned by  $\{\chi_1, \dots, \chi_M\}$ . The entries of the  $M \times M$  matrix  $\mathfrak{T}_M$  are given by  $\mathfrak{T}_{kl,M} = \langle \mathfrak{T}\chi_k, \chi_l \rangle (\mathfrak{m}(J_k))^{-1} = \mathfrak{p}(h^{-1}(J_k), h^{-1}(J_l))$ , where the second equality relies on theorem A. Thus,  $\mathfrak{T}_M$  contains information about the actual transfer operator  $\mathcal{L}$  associated with  $S$ , as induced by  $h$ , and the supplementary coarse-graining induced by the partitioning of  $\mathcal{V}$ .

Note that, because  $\mathfrak{T}$  is a Markov operator, its Galerkin approximation  $\mathfrak{T}_M$  is a row stochastic matrix whose eigenvalues  $\lambda$  satisfy  $|\lambda| \leq 1$ . In the Hamiltonian case of ref. 38,  $\mathfrak{T}$  is self-adjoint and therefore—as  $M$  increases, i.e., the discretization becomes finer—one obtains immediately that the eigenvalues of  $\mathfrak{T}_M$  approximate those of  $\mathfrak{T}$ . For dissipative dynamics, however,  $\mathfrak{T}$  is typically not self-adjoint, and only the dominant eigenvalues of  $\mathfrak{T}$  can be robustly approximated (13, 16). Fortunately, it is the latter we are interested in here, and one can argue that the robustness of the dominant part of the spectrum does apply to the Markov operator  $\mathfrak{T}$  associated with the fJN model (and  $h$ ) (SI Text).

For a given  $M$ , a classical MLE,  $\hat{P}_N$ , can be used to approximate  $\mathfrak{T}_M$  from a given sequence of observations  $\{h(\mathbf{x}_n) : n = 1, \dots, N\}$ , with  $h(\mathbf{x}_n) = \bar{T}_\delta(n\Delta t)$  being the Niño-3 SSTs. The entries of  $\hat{P}_N$  are then simply given by the relative frequencies  $\hat{P}_{kl} = \#\{h(\mathbf{x}_n) \in J_k \wedge h(\mathbf{x}_{n+1}) \in J_l\} / (\#\{h(\mathbf{x}_n) \in J_k\})^{-1}$ , which converge to  $\mathfrak{T}_{kl,M}$  as  $N \rightarrow \infty$  with an error of order  $\mathcal{O}(N^{-1/2})$  (37).

The dynamical interpretation of the Markov operator  $\mathfrak{T}$  given by Eq. 8 and the numerical procedure described above provide a general framework for the estimation from a time series of the spectral gap in the RP resonances, as filtered by a particular observable  $h$ . This spectral RP gap can be estimated from the approximations of the dominant eigenvalues of  $\mathfrak{T}_M$ , whenever the resolution  $M$  of the range of the observations  $x_n$  and the

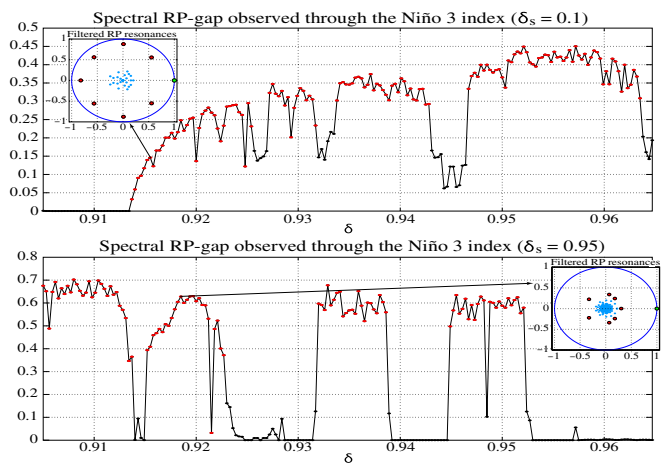


**Fig. 3.** Size  $\tau$  of the spectral RP gap associated with the observable  $h$ , the Niño-3 index from the fJN model, across the parameter range of interest: (Upper) slowly mixing regime and (Lower) rapidly mixing regime. The filtered RP resonances  $\lambda$  appear in the Insets: the eight leading  $\lambda$ s are in red, except the eigenvalue 1, which is in green. The latter corresponds here to the invariant measure  $\mathfrak{m}$  associated with the time 6-mo map. In the slowly mixing regime, the eight leading  $\lambda$ s fall close to the eighth roots of unity (26); they are associated with a near cycle of period 4 for the time 1 map, corresponding to the QQ mode found in the fJN model for this regime (Fig. 2).

number  $N$  of observations are large enough; the statistical errors in these approximations can be estimated by bootstrapping arguments (SI Text). We describe next how the spectral RP gap turns out to be an important factor in the sensitivity of the empirical probability measure that approximates  $m = h_*\mu$ .

### Spectral RP Gap and Sensitivity of Statistical Equilibria

An important result in the stability theory of Markov chains was the discovery of sensitivity bounds relating the stability of a chain and its speed of convergence to equilibrium. Going back to the Markov representation  $\mathfrak{T}$  of the dynamics of the fJN model given by theorem A, we take advantage of the sensitivity bounds for Markov chains to deduce sensitivity properties of the one-dimensional measure  $m = h_*\mu$  that the observable  $h$  extracts from the multidimensional SRB measure  $\mu$ . Out of the many sensitivity bounds in the literature, it is the ones in ref. 40 that are most relevant here.

Recall first that the dual  $\mathfrak{T}^*$  of  $\mathfrak{T}$  defines a transition kernel (41),  $\kappa(x, B) = \mathfrak{T}^* \chi_B(x)$ , which in turn defines a Markov operator  $\mathcal{T}$  on measures  $\nu$  on  $\mathcal{V}$  given by  $\mathcal{T}\nu(B) = \int \kappa(x, B) d\nu(x)$ , for any set  $B$  in the  $\sigma$ -algebra  $\mathcal{B}(\mathcal{V})$  of the observed range of interest  $\mathcal{V}$ . The operators  $\mathcal{T}$  and  $\mathfrak{T}$  are also linked by  $\mathfrak{T}f = (d\mathcal{T}m_f)/dm$ , with  $dm_f = f dm$  for  $f \in L^1_m(\mathcal{V})$  (SI Text). Uniform ergodicity will be the key concept here; it means that the iterates  $\mathcal{T}^n$  of the Dirac measures  $\delta_x$  converge—uniformly in  $x$ —to  $m$  in total variation (TV), i.e., there exists  $\rho < 1$  and  $C < \infty$  such that, for all  $x \in \mathcal{V}$  and all  $n \in \mathbb{Z}^+$ ,  $\|\mathcal{T}^n \delta_x - m\|_{TV} \leq C\rho^n$ .

We now consider perturbations  $\mathcal{P}$  of the Markov operator  $\mathcal{T}$  assumed to obey uniform ergodicity. The main result of ref. 40 stipulates that, if uniform ergodicity holds, then the invariant measure  $\tilde{m}$ , associated with the Markov operator  $\tilde{\mathcal{T}} := \mathcal{T} + \mathcal{P}$ , satisfies the sensitivity bound

$$\|\tilde{m} - m\|_{TV} \leq \left( \theta_C(\rho) + C \frac{\rho^{\theta_C(\rho)}}{1-\rho} \right) \|\mathcal{P}\| := \gamma(\rho, C) \|\mathcal{P}\|, \quad [9]$$

where  $\|\cdot\|$  is the operator norm associated with the total variation norm  $\|\cdot\|_{TV}$  on measures  $m$  in  $\mathcal{V}$  (40). In Eq. 9,  $\theta_C(\rho)$  is the smallest integer greater than or equal to  $-\log(C)/\log(\rho)$ , and  $C \geq 1$  (40).

The smallest  $\rho$  for which geometric ergodicity holds is called the rate of mixing  $\rho_m$  of the Markov chain. For any fixed  $C \geq 1$ ,  $\gamma(\rho, C)$  grows superlinearly to infinity as  $\rho \rightarrow 1$ , allowing in principle a large difference between  $m$  and  $\tilde{m}$ , even for perturbations  $\mathcal{P}$  that are relatively small, as measured by  $\|\mathcal{P}\|$ . The dependence on  $C$  is much weaker, with  $\gamma(\rho, C)$  increasing with  $C$ , but at a sub-linear rate. The size of  $\gamma(\rho, C)$  is thus strongly controlled by  $\rho_m$ .

These results from ref. 40, together with theorem A, allow us to state—for the map  $S$  with SRB measure  $\mu$ , as considered in the previous section—that if the associated Markov operator  $\mathcal{T}$  is uniformly ergodic, then the slower the mixing rate of  $\mathcal{T}$ , i.e., the closer  $\rho_m$  is to 1, the larger we may expect the sensitivity of  $m = h_*\mu$  to be to perturbations of the system. From the dynamic interpretation of RP resonances, we conclude that regimes corresponding to slow decay with pronounced modulations—when observed through a given observable  $h$ —favor rough parameter dependence for the statistics built on  $h$ . These theoretical predictions are confirmed for the fJN model by the numerical calculations that follow.

### Spectral RP Gap for the fJN Model and Sensitivity

Recall that when the state space is finite and 1 is the unique, simple eigenvalue of a stochastic matrix  $P$  on the unit circle, then the mixing rate appearing in Eq. 9 is equal to  $\lambda_2$ , the subdominant eigenvalue of  $P$  (42). When  $\mu$  is mixing, it can be shown that  $\mathfrak{T}_M$  is irreducible and aperiodic, which in turn makes  $\mathfrak{T}_M$  uniformly ergodic (27) such that Eq. 9 can be applied to  $\mathfrak{T}_M$ . We adopt the strategy described above to estimate the gap  $\tau = 1 - |\lambda_2|$  between the unit circle and the subdominant eigenvalue  $\lambda_2$  of  $\mathfrak{T}_M$  and to provide a confidence interval associated with this estimate for each value of  $\delta$ .

Fig. 3 illustrates the use of the spectral gap to quantify the weak and strong mixing regimes discussed earlier. When the gaps observed in the chaotic regimes are compared between the case  $\delta_s = 0.95$  (Lower) and  $\delta_s = 0.1$  (Upper), we find—for each  $\delta$  of interest—that the gap is typically smaller in the latter case than in the former. As a result, a higher sensitivity of the statistics is expected to occur in the case  $\delta_s = 0.1$  according to theorem A and Eq. 9. Recalling the results of Fig. 1, we see that the numerical results in Fig. 3 along with their theoretical interpretations are in very good agreement with the experiments where the highest roughness in the  $\delta$  dependence was observed for the case  $\delta_s = 0.1$ . Even the small regime of sudden changes in SD noted near relative  $\delta$ -values of about 1 in Fig. 1A is consistent with the local decrease in the gap observed in Fig. 3 (Bottom panel), allowing higher sensitivity to occur locally in  $\delta$ . Confidence intervals for these results are provided in the SI Text, supporting their robustness.

From the combination of the theory and numerical results, we infer that the occurrence of rough parameter dependence in the slow mixing case, where the QQ mode is the most energetic, is not a coincidence. This case corresponds to RP resonances that are closer to the imaginary axis than in the rapid mixing case. According to the sensitivity bound of Eq. 9 applied to the Markov representation of the dynamics provided by theorem A, this offers a favorable ground for sensitive behavior to occur.

### Concluding Remarks

This study is a first step in understanding the relationship between the time variability of a dissipative chaotic system and the parameter dependence of its long-term statistics. The relationship between these two aspects via the theory of RP resonances—and the data-based Markov representation developed in this article—opens up a wide range of possible investigations.

In this respect, other interesting Markov representations that have been used in climate dynamics (43–49) might benefit from the framework of RP resonances, given their natural connection with the underlying nonlinear dynamics. In particular, applying RP resonances to the interpretation of metastability and flow regimes in connection to the LfV observed in geophysical flows (1, 44, 45, 50) and their possible role in parameter sensitivity, as well as in linear response theory in the presence of noise (11), are fascinating areas for further exploration.

**ACKNOWLEDGMENTS.** M.D.C. thanks Honghu Liu for help in preparing Fig. S1 and Joyce Meyerson for help in preparing Figs. 1–3. This study was supported by National Science Foundation Grants DMS 1049253 and AGS-1102838, Office of Naval Research Grant N00014-12-1-0911, and Department of Energy Grant DE-SC0006739.

- Ghil M, Chekroun MD, Simonnet E (2008) Climate dynamics and fluid mechanics: Natural variability and related uncertainties. *Physica D* 237(14):2111–2126.
- McWilliams JC (2007) Irreducible imprecision in atmospheric and oceanic simulations. *Proc Natl Acad Sci USA* 104(21):8709–8713.
- Knight CG, et al. (2007) Association of parameter, software, and hardware variation with large-scale behavior across 57,000 climate models. *Proc Natl Acad Sci USA* 104(30):12259–12264.
- Farmer JD (1985) Sensitive dependence on parameters in nonlinear dynamics. *Phys Rev Lett* 55(4):351–354.
- Neelein JD, Bracco A, Luo H, McWilliams JC, Meyerson JE (2010) Considerations for parameter optimization and sensitivity in climate models. *Proc Natl Acad Sci USA* 107(47):21349–21354.
- Gritsun A, Branstator G, Majda A (2008) Climate response of linear and quadratic functionals using the fluctuation-dissipation theorem. *J Atmos Sci* 65(9):2824–2841.
- Lorenz EN (1963) Deterministic non-periodic flow. *J Atmos Sci* 20(2):130–141.
- Reick CH (1996) Linear response functions of chaotic systems and equilibrium moments. *Math Comput Simul* 40(3):281–295.
- Sparrow C (1982) *The Lorenz Equations: Bifurcations, Chaos, and Strange Attractors* (Springer-Verlag, New York).
- Baladi V (2008) Linear response despite critical points. *Nonlinearity* 21(6):81–90.
- Hairer M, Majda A (2010) A simple framework to justify linear response theory. *Nonlinearity* 23(4):909–922.
- Baladi V (2000) *Positive Transfer Operators and Decay of Correlations, Advanced Series Nonlinear Dynamics* (World Scientific, Singapore), Vol 16.

13. Baladi V, Holschneider M (1999) Approximation of nonessential spectrum of transfer operators. *Nonlinearity* 12(3):525–538.
14. Butterley O, Liverani C (2007) Smooth Anosov flows: Correlation spectra and stability. *J. Modern Dynamics* 1(2):301–322.
15. Collet P, Eckmann J-P (2006) *Concepts and Results in Dynamical Systems* (Springer-Verlag, New York).
16. Keller G, Liverani C (1999) Stability of the spectrum for transfer operators. *Annali della Scuola Normale Superiore di Pisa – Classe di Scienze* 28(4):141–152.
17. Lasota A, Mackey MC (1994) *Chaos, Fractals, and Noise: Stochastic Aspects of Dynamics* (Springer, New York), 2nd Ed.
18. Sarig O (2009) *Lecture Notes on Thermodynamic Formalism for Topological Markov Shifts* (Pennsylvania State Univ, State College, PA).
19. Liverani C (2010) On the work and vision of Dmitry Dolgopyat. *J. Modern Dynamics* 4(2):211–225.
20. Pollicott M (1986) Meromorphic extensions of generalized zeta functions. *Invent. Math.* 85(1):147–164.
21. Ruelle D (1986) Resonances of chaotic dynamical systems. *Phys Rev Lett* 56(5):405–407.
22. Ruelle D (1986) Locating resonances for Axiom-A dynamical systems. *J Stat Phys* 44(3-4):281–292.
23. Jin F-F, Neelin JD (1993) Modes of interannual tropical ocean-atmosphere interaction—A unified view. Part I: Numerical results. *J Atmos Sci* 50(21):3477–3503.
24. Jin F-F, Neelin JD, Ghil M (1996) El Niño/Southern Oscillation and the annual cycle: Subharmonic frequency locking and aperiodicity. *Physica D* 98(2):442–465.
25. Zebiak SE, Cane M (1987) A model El Niño–Southern Oscillation. *Mon Weather Rev* 115(10):2262–2278.
26. Dellnitz M, Junge O (1999) On the approximation of complicated dynamical behavior. *SIAM J Numer Anal* 36(2):491–515.
27. Froyland G (1998) Approximating physical invariant measures of mixing dynamical systems in higher dimensions. *Nonlinear Anal* 32(7):831–860.
28. Tziperman E, Cane MA, Zebiak S (1995) Irregularity and locking to the seasonal cycle in an ENSO prediction model as explained by the quasi-periodicity route to chaos. *J Atmos Sci* 52(3):293–306.
29. Jiang N, Neelin JD, Ghil M (1995) Quasi-quadrennial and quasi-biennial variability in the equatorial Pacific. *Clim Dyn* 12(2):101–112.
30. Eckmann J-P, Ruelle D (1985) Ergodic theory of chaos and strange attractors. *Rev Mod Phys* 57(3):617–656.
31. Gallavotti G, Cohen EDG (1995) Dynamical ensembles in stationary states. *J Stat Phys* 80(5-6):931–970.
32. Halmos PR (1974) *Measure Theory* (Springer-Verlag, New York).
33. Constantin P, Kiselev A, Ryzhik L, Zlatos A (2008) Diffusion and mixing in fluid flow. *Ann Math* 168(2):643–674.
34. Froyland G (1997) Computer-assisted bounds for the rate of decay of correlations. *Commun Math Phys* 189(1):237–257.
35. Horvat M, Veble G (2009) A hybrid method for calculation of Ruelle–Pollicott resonances. *J Phys A Math Theor* 42(46):46510.
36. Florido R, Martin-González JM, Gomez Llorente JM (2002) Locating Pollicott–Ruelle resonances in chaotic dynamical systems: A class of numerical schemes. *Phys Rev E Stat Nonlin Soft Matter Phys* 66(4 Pt 2):046208.
37. Billingsley P (1961) *Statistical Inference for Markov Processes* (Univ of Chicago Press, Chicago).
38. Schutte Ch, Fischer A, Huisinga W, Deuffhard P (1999) A direct approach to conformational dynamics based on hybrid Monte Carlo. *J Comput Phys* 151(1):146–168.
39. Chekroun MD, Simonnet E, Ghil M (2011) Stochastic climate dynamics: Random attractors and time-dependent invariant measures. *Physica D* 240(21):1685–1700.
40. Mitrophanov A (2005) Sensitivity and convergence of uniformly ergodic Markov chains. *J Appl Probab* 42(4):1003–1014.
41. Kallenberg O (2002) *Foundations of Modern Probability* (Springer-Verlag, New York).
42. Hennion H, Hervé L (2001) *Limit Theorems for Markov Chains and Stochastic Properties of Dynamical Systems by Quasi-Compactness* (Springer-Verlag, New York).
43. Blumenthal MB (1991) Predictability of a coupled ocean-atmosphere model. *J Clim* 4(8):766–784.
44. Franzke C, Crommelin D, Fischer A, Majda A (2008) A hidden Markov model perspective on regimes and metastability in atmospheric flows. *J Clim* 21:1740–1757.
45. Ghil M, Robertson AW (2002) “Waves” vs. “particles” in the atmosphere’s phase space: A pathway to long-range forecasting? *Proc Natl Acad Sci USA* 99(Suppl 1):2493–2500.
46. Kimoto M, Ghil M (1993) Multiple flow regimes in the Northern Hemisphere winter. Part II: Sectorial regimes and preferred transitions. *J Atmos Sci* 50(16):2645–2673.
47. Mo K, Ghil M (1987) Statistics and dynamics of persistent anomalies. *J Atmos Sci* 44(5):877–901.
48. von Storch H, Bruns T, Fischer-Bruns I, Hasselmann K (1988) Principal oscillation pattern analysis of the 30- to 60-day oscillation in general circulation model equatorial troposphere. *J Geophys Res* 93(D9):11022–11036.
49. Xue Y, Cane MA, Zebiak SE, Blumenthal MB (1994) On the prediction of ENSO: A study with a low-order Markov model. *Tellus* 46A(4):512–528.
50. Berloff PS, McWilliams JC (1999) Large-scale, low-frequency variability in wind-driven ocean gyres. *J Phys Oceanogr* 29(8):1925–1949.

# Supporting Information

Chekroun et al. 10.1073/pnas.1321816111

## SI Text

We provide in this *SI Text* complementary material about (i) the Markov representation obtained in Theorem A and the corresponding numerical results for the forced Jin-Neelin (fJN) model and (ii) the physical formulation of the latter model.

**Markovian Dynamics from Observables.** It is easier to understand the implications of theorem A from a model reduction perspective. This perspective is formulated as corollary B below. We also note here relationships between this framework and various stochastic reduction procedures used so far in climate dynamics.

In particular, we describe how any discrete sequence of observations of a given dissipative, chaotic model in discrete time can be rigorously represented as a particular realization of a Markov process associated with the corresponding observable  $h$ . It is shown that the associated Markov operator  $\mathfrak{L}$ , whose existence is ensured by theorem A, characterizes a coarse-graining—induced by the observable  $h$  in the reduced phase space  $\mathcal{V}$ —of the actual dynamics, along with its transition probabilities.

The reduced Markov models acting on the state space  $\mathcal{V}$  associated with a given observable will be shown to describe the dynamics of the observed variables. This description is given by Markov processes with state-dependent noise that reflects the statistics of the unobserved variables.

We consider in this section a dissipative<sup>†</sup> discrete dynamical system with a bounded nonwandering set  $\Lambda$ , given by  $\mathbf{x}_{n+1} = \mathbf{S}(\mathbf{x}_n)$ , where  $\mathbf{x}_0 \in X = \mathbb{R}^d$ , whereas  $\mathbf{S} : X \rightarrow X$  is a diffeomorphism. The chaotic character of the dynamics is understood in the sense of the existence of a unique ergodic Sinai-Ruelle-Bowen (SRB) measure<sup>‡</sup>  $\mu$ , whose support  $\text{supp}(\mu)$ —i.e., the smallest closed set of full measure for  $\mu$ —is contained in  $\Lambda$  as an invariant measure (6, remark 1.4, p 197);  $\text{supp}(\mu)$  is thus compact because  $\Lambda$  is compact, and it will be denoted by  $\mathfrak{A}$  hereafter.

In the general—i.e., not necessarily chaotic—case and in the applications of interest here, we assume that  $\mathbf{S}$  possesses a unique invariant measure  $\mu$  that is physically relevant in the sense of Eq. S7. By using an analog of Eq. 1 for the discrete-time dynamical system generated by  $\mathbf{S}$ , a transfer operator  $\mathcal{L}$ —acting on probability measures  $\nu$  on  $X$ —can be associated with  $\mathbf{S}$  for any Borel set  $E \subset X$

$$\mathcal{L}\nu(E) := \nu(\mathbf{S}^{-1}(E)), \quad [\text{S1}]$$

where  $\mathbf{S}^{-1}(E) := \{x \in X : \mathbf{S}x \in E\}$ .

For any invariant measure  $\mu$ , whether physical or not, the transfer operator  $\mathcal{L}$  defined in Eq. S1, which acts on measures, can be associated with another transfer operator  $\mathfrak{L}$ , via the

Radon-Nikodym derivative<sup>§</sup> of  $\mathcal{L}\nu$  with respect to  $\mu^{\mathfrak{A}}$ ; this  $\mathfrak{L}$  acts on densities  $f$  with respect to  $\mu$ , according to

$$\mathfrak{L}f := \frac{d\mathcal{L}\nu}{d\mu}, \quad [\text{S2}]$$

for any  $f \in L^1_{\mu}(X)$  such that  $d\nu = f d\mu$  (9). Note that the Radon-Nikodym derivative in Eq. S2 is well defined if  $\mathcal{L}\nu$  is absolutely continuous with respect to  $\mu$ ; the latter condition is satisfied because  $\nu$  has a density with respect to  $\mu$ , and  $\mathbf{S}$  is nonsingular with respect to  $\mu$ . Indeed,  $\mu$  is an invariant measure under  $\mathbf{S}$ , and therefore we naturally have that  $\mu(\mathbf{S}^{-1}(E)) = 0$  if and only if  $\mu(E) = 0$ .

We assume that an observable  $h : X \rightarrow Y$  is given, with  $Y$  a subspace of  $X$  of dimension typically much smaller than that of  $X$ . Having thus clarified the definitions and properties of the objects involved in the statement of theorem A, one can now state the following corollary:

**Corollary B.** *Let  $\mathbf{y}_n := h(\mathbf{x}_n)$ . For any  $\mathbf{y}$  in  $\mathcal{V} = h(\mathfrak{A})$ , let  $\Theta_{\mathbf{y}}$  be the subset of  $\mathfrak{A}$  given by  $h^{-1}(\{\mathbf{y}\}) \cap \mathfrak{A}$ , i.e., the set of  $\mathbf{z}$  in  $\mathfrak{A}$  so that  $h(\mathbf{z}) = \mathbf{y}$ . Then under the assumption of theorem A, the dynamics of the reduced (observed) variables,  $\mathbf{y}_n$  possesses the following representation. There exists a family  $\{\mathcal{M}_{\mathbf{z}} : \mathbf{z} \in \mathfrak{A}\}$  of self-mappings of  $Y$ , and a family  $\{\nu_{\mathbf{y}} : \mathbf{y} \in \mathcal{V}\}$  of probability measures such that  $\text{supp}(\nu_{\mathbf{y}}) \subset \Theta_{\mathbf{y}}$  and*

$$\mathbf{y}_{n+1} = \mathcal{M}_{\mathbf{z}_n}(\mathbf{y}_n), \quad [\text{S3}]$$

where  $\{\mathbf{z}_n\}$  is a sequence of  $\Theta_{\mathbf{y}}$ -valued random elements defined on a probability space  $(\Omega, \mathcal{F}, \mathbb{P})$  such that

$$\mathbb{P}(\mathbf{z}_n \in B | \mathbf{y}_n = \mathbf{y}) = \nu_{\mathbf{y}}(B), \quad [\text{S4}]$$

for any  $\mathbf{y} \in \mathcal{V}$  and any Borel set  $B \in \mathcal{F}$  of  $\Theta_{\mathbf{y}}$ .

This corollary states that, although  $\{\mathbf{x}_n\}$  is generated by iterations of a deterministic map  $\mathbf{S}$ , the sequence of observed variables  $\{\mathbf{y}_n\}$  can be represented as a genuine realization of a Markov chain, when  $\mathbf{S}$  possesses a physical invariant measure in the sense recalled in Eq. S7. The reduced dynamics given by Eq. S3 tells us that when the chain is in the state  $\mathbf{y}$ —i.e., when an observation  $h(\mathbf{x})$  equals  $\mathbf{y}$ —then the future of this state is determined by a map  $\mathcal{M}_{\mathbf{z}}$  that depends on an unobserved variable or hidden state  $\mathbf{z}$ ; according to Eq. S4, this hidden state is sampled from a distribution  $\nu_{\mathbf{y}}$  on  $\Theta_{\mathbf{y}}$ . In general, the  $\nu_{\mathbf{y}}$ s are different for different  $\mathbf{y}$ . The proof of this corollary is constructive and shows that the maps  $\mathcal{M}_{\mathbf{z}}$ , as well as the probability measures  $\nu_{\mathbf{y}}$ , depend on both  $\mathbf{S}$  and its associated invariant physical measure  $\mu$  (see also ref. 10).

Note that, when the evolution in time of the hidden variable  $\mathbf{z}$  is itself governed by a Markov chain and the observed states  $\mathbf{y}$  are drawn from a distribution such as  $\mathcal{N}(\mathbf{v}, \Sigma)$ ,<sup>||</sup> Eq. S3 could reduce

<sup>†</sup>In the sense that there exists a wandering set (1) of positive Lebesgue measure. Such a system is, in particular, not volume preserving. Recall that a wandering set  $W$  is defined as follows:  $W = \{x \in X : \exists U, \text{ a neighborhood of } x, \exists N > 0, \text{ s.t. } \mathbf{S}^n(U) \cap U = \emptyset, \text{ for } n > N\}$ .

<sup>‡</sup>In this article, following refs. 2 and 3, a probability measure  $\mu$  is of SRB type for  $\mathbf{S}$  if it is invariant under  $\mathbf{S}$ , i.e.,  $\mathbf{S}_*\mu = \mu$ ; has a positive Lyapunov exponent, and the conditional measures on the local unstable manifolds (1)—which are contained within the support of  $\mu$ , if  $\mu$  is ergodic (4, theorem 3.2)—are absolutely continuous with respect to the Lebesgue measure on these manifolds (2, definition 6.14). In other words, for any continuous observable  $f$ , an SRB measure can be disintegrated as follows:  $\int f(x) d\mu(x) = \int_{\mathcal{W}^u} d\mu_{\mathcal{W}^u}(w) \int_w f(y) \rho_w(y) d_w(y)$ , where  $\mathcal{W}^u$  is the set of local unstable manifolds,  $d_w y$  is the Lebesgue measure on the local manifold  $w$ ,  $\rho_w$  is a nonnegative density supported by  $w$ , and  $\mu_{\mathcal{W}^u}$  is called the transverse measure. See ref. 5 for additional details.

<sup>§</sup>Roughly speaking, this derivative is analogous to a classical derivative in the calculus of real variables, in the sense that it describes the rate of change of the density of one measure with respect to another (7, 8). A Radon-Nikodym derivative arises implicitly in the use of the Jacobian determinant in classical multivariable integration, which typically appears after a change of variables.

<sup>¶</sup>The operator  $\mathfrak{L}$  describes the action of the dynamics on densities instead of probability measures. The Radon-Nikodym derivative with respect to  $\mu$  allows one to relate these two operators. The definition of  $\mathcal{L}$  does not depend on the invariant measure  $\mu$ . The choice of  $\mu$  determines, however, the action  $\mathfrak{L}$ , defined in Eq. S2, of the dynamics on measures that possess a density with respect to  $\mu$ . To get a meaningful action  $\mathfrak{L}$  on densities depends therefore on how meaningful the invariant measure  $\mu$  is; see Eq. S7.

<sup>||</sup>Here the mean vector  $\mathbf{v}$  and the covariance matrix  $\Sigma$  of this Gaussian measure depend typically on the observed state  $\mathbf{y}$  (11).

to the case of a hidden Markov model (HMM) (11). Several possibilities for the probability laws of  $\mathbf{y}_n$  exist in an HMM modeling perspective. The evolution of these probability laws can, of course, be more general than the usual assumptions used in HMM modeling.

Corollary B helps provide underpinnings for the data-inferred conditional Markov chain approach (12–14) used in stochastic parameterization. In this approach, the unresolved processes are approximated by a Markov chain whose properties depend on the state of the resolved model variables.

When the dynamics is chaotic in the sense recalled above, then  $\nu_y$  as defined in ref. 4 is expected to be absolutely continuous with respect to the Lebesgue measure on the local unstable manifolds that intercept  $\Theta_y$ . As a consequence,  $\nu_y$  is nonsingular and the coarse-grained dynamics—i.e., the dynamics of the observed variables  $\mathbf{y}_n$ —can be naturally interpreted as subject to a state-dependent noise with distribution  $\nu_y$ . Fig. S1 gives a schematic view of the reduced dynamics governed by Eq. S3 in such a case.

Besides the works mentioned above, it is worth noting that the mathematical formulation of reduced dynamics, as provided by corollary B here, is consistent with other, stochastic reduction procedures encountered in the climate dynamics literature or related fields (15–43). Several of these works propose various methods—data based or analytical—to construct in practice reduced models that include state-dependent noise (32, 37, 38) and/or memory effects (18, 19, 25, 29, 33, 37, 38). Essentially, most of these procedures may be viewed as approximating the operator  $\mathcal{M}_{z_n}$  in Eq. S3 and  $\nu_y$  in Eq. S4. These various approximations are discussed in further detail in ref. 10.

**Remark 1.** It is worth mentioning that similar Markov representations of complex dynamics have appeared in various related contexts, such as random billiards (44) or molecular dynamics (45, 46). In ref. 44, the mixing properties of the original system were studied using such Markov representations, and metastability was analyzed in refs. 45 and 46 following a similar approach. The idea of using such representations in the sensitivity analysis of the statistics associated with an arbitrary observable of a dissipative (chaotic) system seems, however, to be new. Note also that, in contradistinction from the cited works, theorem A does not rely on assumptions regarding any randomness inherent to the dynamics (44), nor any kind of reversibility, such as that of Hamiltonian systems (45, 46). In particular, theorem A gives rise to Markov operators  $\mathfrak{T}$  that are typically not self-adjoint for the dissipative systems considered in this article.

**Remark 2.** The Markov operator  $\mathfrak{T}$  ensured by theorem A gives the transition probabilities of the Markov process associated with Eq. S3. This Markov operator possesses another interesting interpretation. For a given function  $\psi \in L^1_{\text{in}}(\mathcal{V})$ ,  $\mathfrak{T}\psi(\mathbf{y})$  provides the expected value of the random variable  $\psi(h \circ \mathbf{S}^{-1}(\mathbf{z}))$ , when  $\mathbf{z}$  is drawn from  $h^{-1}(\{\mathbf{y}\})$  according to the probability law  $\nu_y$  (4). It can be shown then — by a standard application of Jensen’s inequality in a probabilistic setting [8, lemma 2.5], and the fact that  $\mu$  is  $\mathbf{S}$ -invariant—that  $\mathfrak{T}$  also defines a bounded operator on  $L^2_{\text{in}}(\mathcal{V})$ , with  $\text{in}$  being the push-forward\*\* of  $\mu$  by  $h$ . This property is implicitly used in the Galerkin approximation of  $\mathfrak{T}$  described below.

**Filtered Ruelle-Pollicott Resonances.** We explain below how the Ruelle-Pollicott (RP) resonances arise naturally in the decomposition of the autocorrelation function associated with a given observable  $h$ . Recall first that the essential spectral radius  $\rho_*$  of a bounded linear operator acting on a Banach space is the smallest  $\rho > 0$  so that the spectrum of the operator outside the

disk of radius  $\rho$  consists in a finite or countable set of isolated eigenvalues of finite multiplicity (47).

Let now  $\mathcal{L}$  be the transfer operator associated with  $\mathcal{L}$  (Eq. S2). Let us assume that, for some given Banach space  $\mathbf{B}$ , the part  $\sigma_c$  of spectrum of  $\mathcal{L}$  outside a disk of radius  $\theta \in (\rho_*, 1)$  is constituted by a finite number of eigenvalues  $\lambda_i$ , each of finite algebraic multiplicity  $m_i$ . In other words,  $\sigma_c$  is assumed to contain one or more RP resonances and necessarily the dominant ones.

Then, relying on the spectral theory of operators in Banach spaces [48, theorem III-6.17], it can be proved that the following spectral decomposition of  $\mathcal{L}$  holds:

$$\mathcal{L}^n \varphi = \sum_{\lambda_i \in \sigma_c} \left( \psi_i L_i^n \psi_i^* \varphi \right) \lambda_i^n + \mathcal{R} \mathcal{L}^n \varphi, \quad n \in \mathbb{N}, \quad \text{[S5]}$$

where each  $L_i$  is an  $m_i$ -dimensional matrix in Jordan form, each  $\psi_i$  is a row vector taken from a basis of a generalized eigenspace in  $\mathbf{B}$  associated with the RP-resonances  $\lambda_i$ , and each  $\psi_i^*$  is a column vector, with the union of the latter forming a basis of the corresponding generalized eigenspace for  $\mathcal{L}^*$ . When  $\sigma_c$  consists of all of the RP resonances, the operator  $\mathcal{R}$  is the projector associated with the essential part of the spectrum. If now there exists  $C > 0$  such that  $\|\mathcal{R} \mathcal{L}^n\| \leq C \theta^n$ , then Eq. S5 provides a decomposition of  $\mathcal{L}^n$  into a finite-rank operator  $\mathcal{G}_n(\theta)$ , given by the sum over  $\sigma_c$ , and an exponentially decaying correction term  $\mathcal{R} \mathcal{L}^n$ .

A decomposition with the aforementioned properties is known to hold for a broad class of maps or flows on compact manifolds (49–54). For a given observable  $h$  and a Hilbert space  $\mathbf{B} = L^2_\mu(X)$ , to fix the ideas, it can be proved that, if Eq. S5 is satisfied with the decay properties of  $\mathcal{R} \mathcal{L}^n$  mentioned above, then the following decomposition of the autocorrelation function  $\rho_h$  associated with  $h$  holds

$$\rho_h(n) = \sum_{\lambda_i \in \sigma_c} \alpha_n(h) n^{m_i-1} \lambda_i^n + \mathcal{O}(\theta^n). \quad \text{[S6]}$$

Here the coefficients  $\alpha_n(h)$ , which depend on  $h$ , may actually vanish for a certain observable  $h$ .

As a result, a peak in a system’s power spectrum may disappear from observable to observable, depending on how large or small its corresponding coefficient  $\alpha_n$  may be for that  $h$ . A striking example of this dependence on  $h$  is apparent in both observations and simple models of glaciation cycles (55, 56): it involves the difference between the power spectra of regional or local temperatures—as derived from  $\delta\text{O}^{18}$  values in marine-sediment records—and of global ice volume and atmospheric  $\text{CO}_2$  concentration—as derived from  $\delta\text{O}^{18}$  values and from trapped air bubbles in ice cores. A clear instance of this difference can be found by comparing the power spectra of regional air temperature (Fig. 2A) and  $\text{CO}_2$  concentration (Fig. 2C) in the upper 160 ky of the Vostok ice core (57) or by inspecting table 2 from ref. 58; the latter summarizes the spectral lines found to be significant in six marine cores.

By construction, the Markov representation of the reduced dynamics, as described by Eq. S3 in corollary B, captures exactly the RP resonances associated with the nonvanishing coefficients in Eq. S6. The resulting filtered RP resonances then correspond to the eigenvalues of the operator  $\mathfrak{T}$  provided by theorem A.

When some coefficient  $\alpha_k(h)$  dominates the rest of the  $\alpha_n(h)$  s, while the imaginary part  $\omega_k$  of  $\lambda_k$  is nonzero, it corresponds to a near-cycle (54, 59) of period  $\omega_k^{-1}$ . Such a near-cycle occurs for the fJN model in the slowly mixing regime when  $h$  is the Niño-3 index. In that case, a near-cycle of period 4—corresponding to the quasi-quadrennial El Niño–Southern Oscillation (ENSO) mode (60)—can be observed from the estimation of the RP resonances (Fig. 3).

This RP interpretation for the appearance of a spectral peak, as opposed to a sharp line, may differ from the simpler one, given in

\*\*Recall that the push-forward of a probability measure  $\nu$  by a map  $h : X \rightarrow Y$  is defined by  $h_*\nu(E) = \nu(h^{-1}(E))$ , for any Borel set  $E \subset Y$ .

ref. 61, as being due to a weakly unstable periodic orbit. It agrees, on the other hand, with the idea of a “ghost limit cycle” present at a close-by parameter value (62).

**Markov Representations in Practice.** Theorem A and corollary B are particularly useful when the observable  $h$  captures certain key dynamical features of the full dynamics<sup>††</sup> in the reduced phase space  $Y$ . Indeed, as illustrated in the main text and explained below, theorem A allows us to justify that, in practice, the transition probabilities associated with  $h$  can be estimated by a standard maximum likelihood estimator (MLE) (63). More advanced estimation methods could be used (64) but, as shown below, an MLE-based strategy suffices for our purpose of estimating the leading filtered RP resonances for the time series considered in this article.

As in the main text, we assume hereafter that a unique physically relevant invariant measure  $\mu$  exists for the nonlinear time 1 map  $\mathbf{S}$  associated with the truncated version of the fJN model. The time unit is 1 y and the truncation analyzed here is  $d = 408$ .

Recall that an invariant measure  $\mu$  is physical if it can be obtained as a (weak) limit (65) of the empirical measure along the orbit  $\{\mathbf{S}^n \mathbf{x}\}$ ,  $\zeta_N(\mathbf{x}) = \frac{1}{N} \sum_{n=0}^{N-1} (\mathbf{S}^*)^n \delta_{\mathbf{x}}$ , for a Lebesgue-positive set of initial data  $\mathbf{x}$ ; here  $\mathbf{S}^*$  denotes the pullback operator associated with  $\mathbf{S}$  on the space of Borel probability measures.<sup>‡‡</sup> In simpler terms, this property amounts to the statement

$$\lim_{N \rightarrow \infty} \frac{1}{N} \sum_{n=0}^{N-1} f(\mathbf{S}^n \mathbf{x}) = \int f \, d\mu, \quad [\text{S7}]$$

for all real-valued, bounded, continuous functions  $f$  on  $X$  and for  $\mathbf{x} \in B(\mu)$ , with  $B(\mu)$  of positive Lebesgue measure.

In this section, the index  $p$  in theorem A is taken equal to 1,<sup>§§</sup> so that  $\mathcal{V}$  is a subset of the real line. Recall from remark 2 that the operator  $\mathfrak{T}$ —provided by theorem A, as applied to this particular time 1 map  $\mathbf{S}$ —is a well-defined bounded operator on  $L^2_{\text{m}}(\mathcal{V})$ .

**Galerkin Approximations of Markov Operators.** We follow here the approach described in ref. 46 that we adapt to our setting. Let  $\mathcal{V}$  be the projection by  $h$  of the nonwandering set  $\mathfrak{A}$ . We consider, for a given integer  $M$ , the finite state space  $\mathcal{V}_M$  associated with the partition of  $\mathcal{V}$  and given by

$$\mathcal{V} = \bigcup_{k=1}^M U_k, \quad [\text{S8}]$$

where  $U_k \cap U_l = \emptyset$  for  $l \neq k$ . To simplify, we assume the partition to be uniform.

Let  $Q$  be the orthogonal projection, in  $L^2_{\text{m}}(\mathcal{V})$ , onto the space spanned by the characteristic functions  $\chi_{U_j}$ , i.e., the set of step functions that are piecewise constant on the partitioning. More precisely,  $Q$  is defined as follows:

$$Q\varphi = \sum_{j=1}^M \frac{\langle \varphi, \chi_{U_j} \rangle}{\text{m}(U_j)} \chi_{U_j}, \quad \forall \varphi \in L^2_{\text{m}}(\mathcal{V}),$$

where only the terms corresponding to  $\text{m}(U_j) \neq 0$  are taken into account.

<sup>††</sup>For instance, the Niño-3 index used in the main text or the Southern Oscillation index are both well-known observables that capture key features of ENSO variability.

<sup>‡‡</sup>Recall that the pullback of a probability measure  $\nu$  by  $\mathbf{S}$  is defined by  $\mathbf{S}^* \nu(E) = \nu(\mathbf{S}(E))$ , for any Borel set  $E \subset X$ .

<sup>§§</sup>The observable  $h$  here is the Niño-3 index, which is a real-valued function of the phase space.

Let us take  $\psi_i = \frac{\chi_{U_i}}{\text{m}(U_i)}$ , so that  $\{\psi_i\}_{i \in \{1, \dots, M\}}$  forms a basis of probability densities. We have then that

$$Q\mathfrak{T}Q\psi_i = Q\mathfrak{T}\psi_i = \sum_{j=1}^M \frac{\langle \mathfrak{T}\psi_i, \chi_{U_j} \rangle}{\text{m}(U_j)} \chi_{U_j} = \sum_{j=1}^M \frac{\langle \mathfrak{T}\chi_{U_i}, \chi_{U_j} \rangle}{\text{m}(U_j)} \psi_j.$$

Theorem A then yields

$$Q\mathfrak{T}Q\psi_i = \sum_{j=1}^M p(h^{-1}(U_i), h^{-1}(U_j)) \psi_j. \quad [\text{S9}]$$

We will call  $Q\mathfrak{T}Q$  a Galerkin approximation of  $\mathfrak{T}$ , which we denote hereafter by  $\mathfrak{T}_M$ . The problem of computing  $\mathfrak{T}_M$  consists then in determining the  $p(h^{-1}(U_i), h^{-1}(U_j))$  coefficients in Eq. S9 subordinated to the partition (Eq. S8). As explained below, this Galerkin approximation can be performed, in principle, from a time series of  $h(\mathbf{x}_n)$ .

**Galerkin Approximation of  $\mathfrak{T}$  from a Time Series.** Ideally, we should be able to determine first the set  $\mathcal{V} = h(\mathfrak{A})$  to determine  $\mathfrak{T}_M$ . In practice, however, systems of interest have large phase space dimension; here  $d = 408$ , and full climate models have  $d \geq 10^6$ . Thus, it is difficult to directly approximate the nonwandering set  $\mathfrak{A}$  in theorem A and thus  $\mathcal{V}$  from its definition.

From our working assumption on the invariant  $\mu$ , however, the set  $\mathcal{V}$  is sampled according to  $\mu$  by almost<sup>¶¶</sup> any arbitrary time series of observations,  $\{\mathbf{y}_n = h(\mathbf{x}_n) : n = 1, \dots, N\}$ , for a given observable  $h$ , whenever the length  $N$  of the time series is sufficiently large. Recall that  $\mathbf{x}_n = \mathbf{S}^n \mathbf{x}_0$ , where  $\mathbf{S}$  is the time 1 map of our truncated fJN model, initiated in the state  $\mathbf{x}_0 \in \mathbb{R}^d$ , and the dynamics of interest for us is generated by this time 1 map. For the particular case of the Niño-3 index, we thus simply approximate  $\mathcal{V}$  by the empirical interval  $(\min(\mathbf{y}_n), \max(\mathbf{y}_n))$  equipartitioned as in ref. 8, for the given number  $N$  of simulated data points. In what follows, we still denote this interval—along with its corresponding partition—by  $\mathcal{V}$ , as in ref. 8.

We saw in corollary B that the sequence of observations  $\{\mathbf{y}_n\}$ —extracted from a possibly chaotic regime of the fJN model—can be rigorously interpreted as a trajectory of the Markov chain described by Eq. S3. This observation allows justification of

$$p(h^{-1}(U_i), h^{-1}(U_j)) = \mathbb{P}(\mathbf{y}_1 \in U_j | \mathbf{y}_0 \in U_i),$$

because the right side is equal to  $\langle \mathfrak{T}\chi_{U_i}, \chi_{U_j} \rangle / \text{m}(U_j)$ , given the fact that  $\mathfrak{T}$  is also—as explained in remark 2 above—the Markov operator (acting on densities) associated with this Markov chain. The theory of statistical inference for Markov processes (63) can then be simply invoked to determine in practice the probability transition matrix  $P$ , whose entries are given by  $\mathbb{P}(\mathbf{y}_1 \in U_j | \mathbf{y}_0 \in U_i)$ . In what follows, we will identify the matrix  $P$  with the finite-dimensional linear operator  $\mathfrak{T}_M$ .

For a given  $M$ , a classical MLE estimator  $\hat{P}_N$  can then be used to approximate  $\mathfrak{T}_M$  from a time series  $\{\mathbf{y}_n : n = 1, \dots, N\}$ , provided that  $N$  is large enough. A discussion of how large  $N$  needs to be in a practical application follows below. The entries of  $\hat{P}_N$  are then simply given by the relative frequencies

$$\hat{P}_{ij} = \frac{\#\{(\mathbf{y}_n \in U_i) \text{ and } (\mathbf{y}_{n+1} \in U_j)\}}{\#\{\mathbf{y}_n \in U_i\}}.$$

These frequencies converge here to  $p(h^{-1}(U_i), h^{-1}(U_j))$  as  $N \rightarrow \infty$ , with an error of order  $\mathcal{O}(N^{-1/2})$  (63, 64).

<sup>¶¶</sup>In the Lebesgue sense.

**Leading RP Resonances from Time Series.** Given a sufficiently fine discretization of the reduced phase space  $\mathcal{V}$ , and a sufficiently long sequence of observations, one could expect to get a good approximation of the full Markov operator  $\mathfrak{T}$  associated with the observable  $h$ . In particular, its spectrum could also be expected to be well approximated by the spectrum of  $\mathfrak{T}_M$  when  $M$  is sufficiently large. In practice, such strong convergence results are the exception rather than the rule, and a weaker form of convergence is expected to hold, as we explain below.

First note that, because  $\mathfrak{T}$  is a Markov operator, its Galerkin approximation  $\mathfrak{T}_M$  is a row stochastic matrix whose eigenvalues  $\lambda$  lie in the unit disk,  $|\lambda| \leq 1$ . When  $\mathbf{S}$  is energy conserving, it can be shown (45, 46) that  $\mathfrak{T}$  is self-adjoint in  $L^2_{\text{in}}(\mathcal{V})$ , and as  $M$  increases, i.e., when the discretization of the reduced phase space  $\mathcal{V}$  is refined, the entire spectrum of  $\mathfrak{T}_M$  approximates the spectrum of  $\mathfrak{T}$ . We cannot, however, expect this to be so here, because  $\mathfrak{T}$  is typically not self-adjoint for dissipative dynamics, which is the case for the time 1 map of any truncation of the fJN model in certain regimes.

Indeed, as proven in refs. 47 and 66 for a broad class of dynamical systems, only the isolated (discrete) part of the spectrum can be expected to be robustly approximated. These theoretical results support the idea that the dominant part (in modulus) of  $\sigma(\mathfrak{T})$  can be expected to be well approximated when sufficient statistics are available for sufficiently large  $M$ .

The rate of convergence as  $M$  increases is, however, difficult to estimate and will be addressed elsewhere. We describe for the moment how to quantify the uncertainty in the estimation of the dominant part of  $\sigma(\mathfrak{T}_M)$ , as obtained from the MLE procedure described above.

**Confidence Intervals for RP Gaps from Time Series.** We now turn to the problem of quantifying uncertainty in the estimation of the RP gaps from the time series and of constructing associated confidence intervals. For this purpose, we use a bootstrap approach (67) adapted to our framework.

The first step consists of building other possible data sets of the same size as the original data, by drawing with replacement from the original data set. In our case, this is performed by addressing, separately, each row of the transition count matrix,  $C = \{C_{ij}\}_{i,j \in \{1, \dots, M\}}$ , with

$$C_{ij} = \#\{(h(\mathbf{x}_n) \in U_i) \text{ and } (h(\mathbf{x}_{n+1}) \in U_j)\}, \quad [\text{S10}]$$

where  $U_i$  and  $U_j$  are sets defined in partition (8). In other words the entry  $C_{ij}$  gives the total number of transition samples, which—as observed through  $h$ —start in  $U_i$  and end up in  $U_j$ , after one iteration of  $\mathbf{S}$  or, equivalently, after one iteration of the Markov chain given by Eq. S3.

Let  $n_i$  denote the total number of transitions for row  $i$  of the matrix  $C$ . Bootstrapping row  $i$  simply involves sampling  $n_i$  transitions with replacement from the observed  $n_i$  transitions. In other words,  $n_i$  draws are taken from a multinomial distribution with a 1-by- $N$  vector of probabilities  $\{\hat{P}_{il} : l = 1, \dots, N\}$  to generate a new set of transition counts for row  $i$ . Combining the results of each row forms a new transition count matrix  $D$  and thus another possible transition probability matrix  $\hat{Q}_N$ . The collection of bootstrapped transition matrices approximates the sampling distribution.

From this distribution, one can assess the uncertainty of each entry in  $\hat{P}_N$ , as estimated by the MLE procedure, as well as any function of this matrix, like the spectral gap between 1 and the rest of the spectrum. By computing the RP gap for each matrix in the bootstrap set, we create a sampling distribution for RP gaps and then compute the confidence intervals associated with this distribution.

The corresponding results on the robustness of the spectral RP gaps estimated from the Niño-3 index of fJN model simulations are reported in Fig. S2 for the slowly mixing regime considered in Fig. 3. Recall that the estimates here are based on a time series of length 8,800 y, which are sampled every 6 mo<sup>\*\*\*</sup>; thus,  $N = 17,600$ . The resolution of the discretization of  $\mathcal{V}$  is given by  $M = 128$  bins.

The results in Fig. S2 show that the spectral RP gaps presented in Fig. 3 are estimated quite robustly. In agreement with the theoretical predictions of refs. 47 and 66, the smallest RP gaps are associated in Fig. S2 with the smallest error bars. This numerical confirmation is quite reassuring, because it guarantees that an RP gap is best estimated at parameter values at which it is the most important for assessing the model's overall parameter sensitivity.

**Interpretation of the Sensitivity Bound (Eq. 9).** We provide here complementary information regarding the sensitivity bound in Eq. 9. This bound was applied to  $\mathfrak{T}_M$  in the main text. The corresponding Markov chain acts then on a finite-state space associated with a finite partition, as specified in Eq. S8.

When the invariant measure  $\mu$  of system  $\mathbf{S}$  is mixing, it can be shown, using theorem A and arguments similar to those in ref. 68, that  $\mathfrak{T}_M$  is irreducible and aperiodic. The theory of finite-state Markov chains ensures then that  $\mathfrak{T}_M$  is uniformly ergodic (69, theorem 4.9).

Recall that the total variation (TV) distance between probability measures used in Eq. 9 can be defined as

$$\|\tilde{\mathfrak{m}} - \mathfrak{m}\|_{\text{tv}} = \sup_{A \in \mathcal{B}} |\tilde{\mathfrak{m}}(A) - \mathfrak{m}(A)|, \quad [\text{S11}]$$

where  $\mathcal{B}$  is the  $\sigma$ -algebra generated by the partition  $\{U_k : k = 1, \dots, M\}$  in Eq. S8 (69, chapter 4). From ref. 11, we infer that  $\|\tilde{\mathfrak{m}} - \mathfrak{m}\|_{\text{tv}}$  gives the largest possible difference between the probabilities that  $\tilde{\mathfrak{m}}$  and  $\mathfrak{m}$  can assign to the same event  $A$ . The total variation (TV) distance between two probability measures is then equal to 1 if and only if the two measures are mutually singular.

In the general case, the TV distance between two probability measures is determined by their overlap in the following sense. If  $\tilde{\mathfrak{m}}$  and  $\mathfrak{m}$  have densities  $\mathcal{D}_{\tilde{\mathfrak{m}}}$  and  $\mathcal{D}_{\mathfrak{m}}$  with respect to some common reference measure<sup>†††</sup>  $\nu$ , then the following equivalent characterization of the TV distance holds (70)

$$\|\tilde{\mathfrak{m}} - \mathfrak{m}\|_{\text{tv}} = \int |\mathcal{D}_{\tilde{\mathfrak{m}}}(x) - \mathcal{D}_{\mathfrak{m}}(x)| d\nu(x). \quad [\text{S12}]$$

Using the notion of coupling between probability distributions (69), another interesting probabilistic interpretation can be associated with the partition (Eq. S8): it measures how close to indistinguishable (8, p 34) two random variables  $\tilde{\mathbf{y}}$  and  $\mathbf{y}$ —generated with invariant distributions  $\tilde{\mathfrak{m}}$  and  $\mathfrak{m}$ <sup>†††</sup>—are, when seen through the coarse-graining of the partition (Eq. S8) (69, proposition 4.7).

The sensitivity bound provided in Eq. 9, along with the numerical estimation of the RP gaps reported there, lead then to an interesting interpretation. For a given observable  $h$ , the smaller the filtered RP gap of an unperturbed system  $\mathbf{S}$ , the more the system can be expected to have sample paths of the reduced dynamics (3) that differ with high probability from those of the reduced dynamics associated with a perturbed  $\tilde{\mathbf{S}}$ . Furthermore, the sample paths of the reduced dynamics, associated, respectively, with  $\mathbf{S}$  and  $\tilde{\mathbf{S}}$ , will be distributed according to distributions whose nonoverlapping regions are likely to become more and more significant.

\*\*\*As used for Fig. 3.

†††We can always take  $\nu = \frac{1}{2}(\tilde{\mathfrak{m}} + \mathfrak{m})$ .

†††More precisely,  $\|\tilde{\mathfrak{m}} - \mathfrak{m}\|_{\text{tv}} = \inf \{\mathbb{P}(\tilde{\mathbf{y}} \neq \mathbf{y})\}$ , where  $\tilde{\mathbf{y}}$  and  $\mathbf{y}$  have distributions  $\tilde{\mathfrak{m}}$  and  $\mathfrak{m}$ , respectively.

**Intermediate-Complexity ENSO Model.** A brief recapitulation of the JN model description is provided here for the reader's convenience; see refs. 71–74 for details of the autonomous unforced model and refs. 75–78 for versions including the seasonal forcing (79).

**Ocean.** The ocean dynamics is described by linear shallow-water equations for the currents and a nonlinear equation for the sea-surface temperature (SST). The dynamical variables are the three velocity components,  $(u, v, w)$ , and the thermocline depth anomaly  $h$ . The parameters of the corresponding model described below are those of table 1 from ref. 78 except for the values of  $\delta$  and  $\delta_s$ , which have been prescribed according to the experiments reported in the main text, and the value of the coupling parameter  $\mu$  has been set to 1.4.

**SST equation.** The SST in an equatorial band is modeled as satisfying

$$\begin{aligned} \frac{\partial T}{\partial t} + u_1 \frac{\partial T}{\partial x} + \mathcal{H}(w) \frac{w}{H_{1.5}} (T - T_{\text{sub}}(h)) - \mathcal{H}(-v_N) \frac{2v_N}{L_y} (T - T_N) \\ + \epsilon_T (T - T_0) = 0, \end{aligned} \quad [\text{S13}]$$

where  $T$  is the temperature of the surface mixed layer,  $u_1$  (respectively,  $w$ ) is the zonal (respectively, vertical) velocity in this surface layer, and  $v_N$  the meridional surface current at the northern boundary of the equatorial box. Symmetry of SST and anti-symmetry of  $v_N$  are assumed.

In Eq. S13, the Newtonian damping time is denoted by  $\epsilon_T$ , and its value is set at  $(90 \text{ d})^{-1}$ ,  $L_y$  denotes the width of the box, and  $T_N$  is the off-equatorial SST at a distance  $L_y$  from the equator. The depths  $H_1$  and  $H_2$  of the two layers are taken here to be 50 and 100 m, whereas  $H_{1.5} = 75 \text{ m}$  is the depth scale that characterizes upwelling of the subsurface temperature  $T_{\text{sub}}$ .

An analytical, smooth version  $\mathcal{H}(x)$  of the Heaviside function  $H(x)$

$$H(x) = \begin{cases} 1 & \text{if } x > 0 \\ 0 & \text{if } x \leq 0 \end{cases}, \quad [\text{S14}]$$

is used in the terms of Eq. S13 representing upstream differencing of meridional and vertical advection into the equatorial-surface strip.

The meridional velocity  $v_N$  is obtained by finite differencing of the following continuity equation:

$$2 \frac{v_N}{L_y} = \frac{w}{H_1} - \frac{\partial u_1}{\partial x}, \quad [\text{S15}]$$

where  $w$  and  $u_1$  are a sum of three parts: climatological annually varying basic state, anomalous vertical mean currents above the thermocline obtained from shallow-water equations (Eqs. S27 and S28), and anomalous oceanic shear currents determined from Eqs. S32, S37, and S38.

The subsurface temperature  $T_{\text{sub}}$  is parameterized as a nonlinear function of thermocline depth anomaly  $h$  such that a deeper thermocline is associated with warmer upwelled waters resulting in the relation

$$T_{\text{sub}}(h) = T_{s0} + (T_0 - T_{s0}) \tanh\left(\frac{h + h_0}{h_*}\right), \quad [\text{S16}]$$

where the equilibrium value  $T_0$  of SST is set at  $29^\circ \text{C}$ , oceanic temperature at thermocline layer  $T_{s0} = 20^\circ \text{C}$ ,  $h_0 = 40 \text{ m}$ ,  $h_* = 25 \text{ m}$ .

**Oceanic currents.** The vertical-mean motions above the thermocline are governed by the linearized reduced-gravity shallow-water equations on a  $\beta$ -plane in the long-wave approximation

$$\delta \frac{\partial u}{\partial t} - \beta y v + \epsilon u = -g \frac{\partial h}{\partial x} + \frac{\tau}{\rho H}, \quad [\text{S17}]$$

$$\beta y u = -g \frac{\partial h}{\partial y}, \quad [\text{S18}]$$

$$\delta \frac{\partial h}{\partial t} + H \left( \frac{\partial u}{\partial x} + \frac{\partial v}{\partial y} \right) + \epsilon h = 0. \quad [\text{S19}]$$

Here,  $\tau$  is the zonal wind stress,  $\rho$  is the oceanic density,  $H = H_1 + H_2$  is the total depth of the two layers, and  $\epsilon = (2.5 \text{ y})^{-1}$  is the damping rate for the vertical-mean currents. The relative adjustment time coefficient  $\delta$  measures the ratio of the time scale of adjustment by oceanic dynamics to the net time scale of SST change through the SST equation. This parameter affects the travel time of the equatorially trapped waves produced by the model, an essential feature in the physics of the model. From a modeling point of view, this parameter is subject to adjustment through a certain range associated with uncertainty in its estimate and is therefore a natural candidate for a parameter dependence analysis such as performed in the main text.

The usual boundary conditions for the shallow-water equations in the long-wave approximation are used

$$u = 0 \text{ at } x = x_E, \quad [\text{S20}]$$

$$\int_{-\infty}^{\infty} u dy = 0 \text{ at } x = x_W, \quad [\text{S21}]$$

where  $x_E$  and  $x_W$  locate the eastern and western boundaries, respectively.

Given the linear change of variables

$$q = h + u, \quad [\text{S22}]$$

$$r = h - u, \quad [\text{S23}]$$

the shallow-water equations can be rewritten as

$$\left( \delta \frac{\partial}{\partial t} + \epsilon \right) q - yv + \frac{\partial q}{\partial x} + \frac{\partial v}{\partial y} = \tau, \quad [\text{S24}]$$

$$\left( \delta \frac{\partial}{\partial t} + \epsilon \right) r + yv - \frac{\partial r}{\partial x} + \frac{\partial v}{\partial y} = -\tau, \quad [\text{S25}]$$

$$yq - yr + \frac{\partial q}{\partial y} + \frac{\partial r}{\partial y} = 0, \quad [\text{S26}]$$

where all of the variables are nondimensional.

A standard semispectral discretization is used, with parabolic cylinder functions as the basis functions in latitude, leading to a truncated model including the first Kelvin mode and the first 15 symmetric Rossby modes. Note that this represents a higher resolution than typically used for this model (72, 75–77), where a total of eight ocean modes were retained.

The resulting equations for the oceanic wave coefficients  $q_n$  read as follows:

$$\left( \delta \frac{\partial}{\partial t} + \epsilon \right) q_0 + \frac{\partial q_0}{\partial x} = \tau_0, \quad [\text{S27}]$$

and for  $n \in \{2p, p \in \{1, \dots, 15\}\}$ ,

$$(n-1) \left( \delta \frac{\partial}{\partial t} + \epsilon \right) q_n - \frac{\partial q_n}{\partial x} = n\tau_n - [(n-1)]^{1/2} \tau_{n-2}, \quad [\text{S28}]$$

where  $\tau_n$  is the zonal wind stress projected onto oceanic mode  $n$ ,  $q_0$  is the amplitude of the Kelvin wave, and the  $q_n$  s for  $n = 2, 4, \dots, 30$ , are the amplitudes of the first 15 Rossby waves. The original variables  $h$ ,  $u$ , and  $v$  are obtained by back transformation as appropriate linear combination of  $q_n$  s, thus obtaining thermocline depth anomalies and anomalous vertical mean currents above the thermocline.

Equations for mean zonal currents (Eqs. S27 and S28) and SST (Eq. S13) are numerically discretized using 24 grid points on the equator, which gives in total  $(16+1) \times 24 = 408$  degrees of freedom.

Note that the surface layer zonal (respectively, meridional) velocity  $u_1$  (respectively,  $v_1$ <sup>§§§</sup>) of Eq. S13 is decomposed as  $u_1 = u + u_s$  (respectively,  $v_1 = v + v_s$ ), where  $u_s$  (respectively,  $v_s$ ) represents the zonal (respectively, meridional) contribution coming from the vertical shear currents.

The horizontal components  $u_s$  and  $v_s$  of the vertical-shear currents are governed by steady-state equations dominated by damping due to interfacial stress between the layers (79)

$$\epsilon_s u_s - \beta y v_s = \frac{\tau H_2}{\rho H_1 H}, \quad [\text{S29}]$$

$$\epsilon_s v_s + \beta y u_s = 0, \quad [\text{S30}]$$

where  $\epsilon_s = (2 \text{ d})^{-1}$  is the damping coefficient for the shear currents.

The vertical velocity in the surface layer,  $w$  in Eq. S13, is also decomposed as  $w = w_s$ . The vertical component  $w_s$  of the shear currents can be calculated from the continuity equation using  $u_s$  and  $v_s$

$$w_s = H_1 \left( \frac{\partial u_s}{\partial x} + \frac{\partial v_s}{\partial y} \right). \quad [\text{S31}]$$

For simplicity, the three components of the shear current are written as

$$u_s = b_u \tau, \quad v_s = -\frac{L_y}{2H_1} b_w \frac{\tau}{\rho H}, \quad w_s = -b_w \tau + H_1 b_u \frac{\partial \tau}{\partial x}, \quad [\text{S32}]$$

where  $b_u \approx H_2/H_1 \epsilon_s$  and  $b_w \approx (H_1/L_d) b_u$ , and  $L_d$  is the characteristic meridional length scale determined by the damping time scale of vertical mixing:  $L_d \equiv \epsilon_s/\beta$ .

**Atmosphere.** The steady response of the zonal wind-stress anomalies  $\tau'$  to SST anomalies  $T'$  at the equator is

$$\tau'(x, 0) = \mu A \left[ \frac{3}{2} e^{3\epsilon_a x} \int_x^{x_E} T'(s) e^{-3\epsilon_a s} ds - \frac{1}{2} e^{\epsilon_a x} \int_{x_W}^x T'(s) e^{\epsilon_a s} ds \right]. \quad [\text{S33}]$$

<sup>§§§</sup>In fact, only the value  $v_N$  of  $v_1$  at the northern boundary of the equatorial box is needed in Eq. S13.

1. Guckenheimer J, Holmes P (1991) *Nonlinear Oscillations, Dynamical Systems and Bifurcations of Vector Fields* (Springer-Verlag, New York), 2nd Ed.
2. Collet P, Eckmann J-P (2006) *Concepts and Results in Dynamical Systems* (Springer-Verlag, New York).
3. Young L-S (2002) What are SRB measures, and which dynamical systems have them? *J Stat Phys* 108(5):733–754.
4. Hatomoto J (2007) Ergodic measures of SRB attractors. *Tokyo J Math* 30(1):257–282.
5. Ledrappier F, Young LS (1985) The metric entropy of diffeomorphisms: I. Characterization of measures satisfying Pesin's formula; II. Relations between entropy, exponents and dimension. *Ann Math* 122(3):509–539.

Here  $A$  is an amplitude factor,  $\epsilon_a$  is a Rayleigh friction due to boundary layer turbulence, and  $\mu$  is an ocean-atmosphere coupling parameter.

**Climatological state and coupling.** The climatological basic state with an annual cycle is constructed as a forced solution of the uncoupled ocean model. The oceanic component is then coupled with the atmospheric model for the deviations from this basic state (referred to as anomalies). The following smooth function that resembles the annually varying observed wind stress in the Pacific along the equator is used to set up the basic state

$$\bar{\tau} = 0.6 \left[ 0.12 - \cos^2 \left( \frac{\pi(x-x_0)}{2x_0} \right) \right] \left[ 1 + \frac{1}{2} \sin \left( \frac{2\pi t}{T_a} \right) \right], \quad [\text{S34}]$$

with  $x_0 = 0.57L$ , where  $L$  is the basin width, and  $T_a = 12$  mo.

The coupled system is set up using one-way flux correction (72), with total wind stress  $\tau$  given by

$$\tau = \bar{\tau} + \tau', \quad [\text{S35}]$$

where the wind stress anomaly  $\tau'$  is derived from the atmospheric response to SST anomalies  $T'$

$$T' = T - \bar{T}, \quad [\text{S36}]$$

according to Eq. S33. The feedback between the ocean and atmosphere takes place every time step.

**Parameter  $\delta_s$ .** A relative surface-layer parameter  $\delta_s$ , varying from unity zero, is introduced that controls the intensity of the anomalous surface-layer currents as a function of the wind-stress anomalies without affecting the climatology. For sensitivity studies in related systems using this parameter, see refs. 71, 72, and 76. Here, this parameter is used at low and high values because it turns out that the respective regimes thus accessed are associated with different mixing properties (within the phase space) of the system when the latter exhibits chaotic behavior. For  $\delta_s$  close to 0, slower decay of correlations of the simulated Niño-3 index tends to occur than for small values of  $\delta_s$ .

The horizontal  $u_s$  and  $v_s$  and vertical  $w_s$  components from the vertical-shear currents are then given by

$$u_s = \bar{u}_s, \quad v_s = \bar{v}_s + \delta_s v'_s, \quad w_s = \bar{w}_s + \delta_s w'_s. \quad [\text{S37}]$$

Here  $\bar{u}_s, \bar{v}_s, \bar{w}_s$  are the velocity components obtained by using the climatological annually varying wind stress (Eq. S34) in Eq. S32, whereas  $v'_s, w'_s$  are shear (surface-layer) currents associated with the anomalous coupling

$$w'_s = -b_w \tau' + H_1 b_u \frac{\partial \tau'}{\partial x}, \quad v'_s = -b_w \tau'. \quad [\text{S38}]$$

Note that  $u_s$  does not depend on  $\delta_s$  (77, 78), a choice made for clarity of the physical mechanisms involved, i.e., controlling only the strength of the anomalous surface meridional cell induced by the wind stress anomalies.

6. Foias C, Manley O, Rosa R, Temam R (2001) *Navier-Stokes Equations and Turbulence. Encyclopedia of Mathematics and Its Applications* (Cambridge Univ Press, Cambridge, UK), Vol 83.
7. Halmos PR (1974) *Measure Theory* (Springer-Verlag, New York).
8. Kallenberg O (1997) *Foundations of Modern Probability* (Springer-Verlag, New York).
9. Sarig O (2009) *Lecture Notes on Thermodynamic Formalism for Topological Markov Shifts* (Pennsylvania State University, State College, PA).
10. Darve E, Solomon J, Kia A (2009) Computing generalized Langevin equations and generalized Fokker-Planck equations. *Proc Natl Acad Sci USA* 106(27):10884–10889.

11. Franzke C, Crommelin D, Fischer A, Majda AJ (2008) A hidden Markov model perspective on regimes and metastability in atmospheric flows. *J Clim* 21(8):1740–1757.
12. Crommelin D, Vanden Eijnden E (2008) Subgrid-scale parametrization with conditional Markov chains. *J Atmos Sci* 65(8):2661–2675.
13. Dorrestijn J, Crommelin D, Siebesma AP, Jonker HJJ (2013) Stochastic parameterization of shallow cumulus convection estimated from high-resolution model data. *Theor Comput Fluid Dyn* 27(1–2):133–148.
14. Nimsaila K, Timofeyev I (2010) Markov chain stochastic parameterizations of essential variables. *Multiscale Model Simul* 8(5):2079–2096.
15. Abramov RV (2013) A simple closure approximation for slow dynamics of a multiscale system: Nonlinear and multiplicative coupling. *Multiscale Model Simul* 11(1):134–151.
16. Blumenthal MB (1991) Predictability of a coupled ocean-atmosphere model. *J Clim* 4(8):766–784.
17. Buizza R, Miller M, Palmer T (1999) Stochastic representation of model uncertainty in the ECMWF Ensemble Prediction System. *Q J R Meteorol Soc* 125(560):2887–2908.
18. Chekroun MD, Kondrashov D, Ghil M (2011) Predicting stochastic systems by noise sampling, and application to the El Niño–Southern Oscillation. *Proc Natl Acad Sci USA* 108(29):11766–11771.
19. Chorin AJ, Hald OH, Kupferman R (2002) Optimal prediction with memory. *Physica D* 166(3):239–257.
20. Fatkullin I, Vanden-Eijnden E (2004) A computational strategy for multiscale systems with applications to Lorenz 96 model. *J Comput Phys* 200(2):605–638.
21. Frank FE, Gottwald GA (2013) Stochastic homogenization for an energy conserving multi-scale toy model of the atmosphere. *Physica D* 254(1):46–56.
22. Givon D, Kupferman R, Stuart A (2004) Extracting macroscopic dynamics: Model problems and algorithms. *Nonlinearity* 17(6):R55–R127.
23. Hasselmann K (1976) Stochastic climate models: Part I. Theory. *Tellus* 28:473–485.
24. Khouider B, Majda AJ, Katsoulakis MA (2003) Coarse-grained stochastic models for tropical convection and climate. *Proc Natl Acad Sci USA* 100(21):11941–11946.
25. Kondrashov D, Chekroun MD, Robertson AW, Ghil M (2013) Low-order stochastic model and “past-noise forecasting” of the Madden-Julian Oscillation. *Geophysical Research Letters* 40(19):5305–5310.
26. Kondrashov D, Kravtsov S, Robertson AW, Ghil M (2005) A hierarchy of data-based ENSO models. *J Clim* 18(21):4425–4444.
27. Kravtsov S, Kondrashov D, Ghil M (2005) Multilevel regression modeling of nonlinear processes: Derivation and applications to climatic variability. *J Clim* 18(21):4404–4424.
28. Kravtsov S, Kondrashov D, Ghil M (2009) *Empirical Model Reduction and the Modeling Hierarchy in Climate Dynamics, Stochastic Physics and Climate Modeling*, eds Palmer TN, Williams P (Cambridge Univ Press, Cambridge, UK), pp 35–72.
29. Majda AJ, Harlim J (2013) Physics constrained nonlinear regression models for time series. *Nonlinearity* 26(1):201–217.
30. Majda AJ, Franzke Ch, Khouider B (2008) An applied mathematics perspective on stochastic modelling for climate. *Phil Trans R Soc A* 366(1875):2427–2453.
31. Majda AJ, Khouider B (2002) Stochastic and mesoscopic models for tropical convection. *Proc Natl Acad Sci USA* 99(3):1123–1128.
32. Majda AJ, Timofeyev I, Vanden-Eijnden E (2001) A mathematical framework for stochastic climate models. *Commun Pure Appl Math* 54(8):891–974.
33. McWilliams JC (2012) The elemental shear dynamo. *J Fluid Mech* 699:414–452.
34. Penland C (1989) Random forcing and forecasting using principal oscillation pattern analysis. *Mon Weather Rev* 117(10):2165–2185.
35. Penland C, Sardeshmukh PD (1995) The optimal growth of tropical sea surface temperature anomalies. *J Clim* 8(8):1999–2024.
36. Stinis P (2006) A comparative study of two stochastic mode reduction methods. *Physica D* 213(2):197–213.
37. Wouters J, Lucarini V (2013) Multi-level dynamical systems: Connecting the Ruelle response theory and the Mori-Zwanzig Approach. *J Stat Phys* 151(5):850–860.
38. Wouters J, Lucarini V (2012) Disentangling multi-level systems: Averaging, correlations and memory. *J Stat Mech Theory Experiment* 2012(03):P03003.
39. Xue Y, Cane MA, Zebiak SE, Blumenthal MB (1994) On the prediction of ENSO: A study with a low-order Markov model. *Tellus* 46A(4):512–528.
40. Zhang Y, Held IM (1999) A linear stochastic model of a GCMs midlatitude storm tracks. *J Atmos Sci* 56(19):3416–3435.
41. von Storch H, Bruns T, Fischer-Brunns I, Hasselmann K (1988) Principal oscillation pattern analysis of the 30- to 60-day oscillation in general circulation model equatorial troposphere. *J Geophys Res* 93(D9):11022–11036.
42. Franzke C, Majda AJ, Vanden-Eijnden E (2005) Low-order stochastic model reduction for a realistic barotropic model climate. *J Atmos Sci* 62(6):1722–1745.
43. Pavliotis GA, Stuart AM (2008) *Multiscale Methods: Averaging and Homogenization, Texts in Applied Mathematics* (Springer, New York).
44. Feres R, Zhang H-K (2012) Spectral gap for a class of random billiards. *Commun Math Phys* 313(2):479–515.
45. Schütte Ch (1999) *Conformational dynamics: Modelling, theory, algorithm, and application to biomolecules*, Habilitation thesis (Fachbereich Mathematik und Informatik, Freie Universität Berlin, Berlin).
46. Schütte Ch, Fischer A, Huisinga W, Deuffhard P (1999) A direct approach to conformational dynamics based on hybrid Monte Carlo. *J Comput Phys* 151(1):146–168.
47. Baladi V, Holschneider M (1999) Approximation of nonessential spectrum of transfer operators. *Nonlinearity* 12(3):525–538.
48. Kato T (1995) *Perturbation Theory for Linear Operators* (Springer-Verlag, Berlin).
49. Baladi V (1998) Periodic orbits and dynamical spectra. *Ergodic theory and dynamical systems* 18(2):255–292.
50. Butterley O, Liverani C (2007) Smooth Anosov flows: Correlation spectra and stability. *J. Modern Dynamics* 1(2):301–322.
51. Dolgopyat D (1998) On decay of correlations in Anosov flows. *Ann Math* 147(2):357–390.
52. Faure F, Tsujii M (2013) Band structure of the Ruelle spectrum of contact Anosov flows. *C R Math* 351(9–10):385–391.
53. Liverani C (2010) On the work and vision of Dmitry Dolgopyat. *J. Modern Dynamics* 4(2):211–225.
54. Melbourne I, Gottwald GA (2008) Power spectra for deterministic chaotic dynamical systems. *Nonlinearity* 21(1):179–189.
55. Ghil M (1994) Cryothermodynamics: The chaotic dynamics of paleoclimate. *Physica D* 77(1):130–159.
56. Ghil M, Childress S (1987) *Topics in Geophysical Fluid Dynamics: Atmospheric Dynamics, Dynamo Theory and Climate Dynamics* (Springer-Verlag, New York).
57. Yiou P, et al. (1991) High-frequency paleovariability in climate and CO<sub>2</sub> levels from Vostok ice-core records. *J Geophys Res* 96(B12):20365–20378.
58. Yiou P, Ghil M, Jouzel J, Paillard D, Vautard R (1994) Nonlinear variability of the climatic system, from singular and power spectra of late Quaternary records. *Clim Dyn* 9(8):371–389.
59. Dellnitz M, Junge O (1999) On the approximation of complicated dynamical behavior. *SIAM J Numer Anal* 36(2):491–515.
60. Jiang N, Neelin JD, Ghil M (1995) Quasi-quadrennial and quasi-biennial variability in the equatorial Pacific. *Clim Dyn* 12(2):101–112.
61. Ghil M, et al. (2002) Advanced spectral methods for climatic time series. *Rev Geophys* 40(1):3–3.41.
62. Kimoto M, Ghil M (1993) Multiple flow regimes in the Northern Hemisphere winter. Part II: Sectorial regimes and preferred transitions. *J Atmos Sci* 50(16):2645–2673.
63. Billingsley P (1961) *Statistical Inference for Markov Processes* (Univ of Chicago Press, Chicago).
64. Crommelin D, Vanden-Eijnden E (2006) Fitting time series by continuous-time Markov chains: A quadratic programming approach. *J Comput Phys* 217(2):782–805.
65. Billingsley P (1999) *Convergence of Probability Measures* (Wiley, New York), 2nd Ed.
66. Keller G, Liverani C (1999) Stability of the spectrum for transfer operators. *Ann Scuola Norm Sup Pisa. Clin Sci* XXVIII(4):141–152.
67. Efron B, Tibshirani RJ (1993) *An Introduction to the Bootstrap* (Chapman & Hall, New York).
68. Froyland G (1998) Approximating physical invariant measures of mixing dynamical systems in higher dimensions. *Nonlinear Anal* 32(7):831–860.
69. Levin DA, Peres Y, Wilmer EL (2008) *Markov Chains and Mixing Times* (American Mathematical Society, Providence, RI).
70. Ambrosio L, Gigli N, Savaré G (2008) *Gradient Flows in Metric Spaces and in the Space of Probability Measures, Lectures in Mathematics ETH Zürich* (Birkhäuser, Basel), 2nd Ed.
71. Neelin JD (1991) The slow sea surface temperature mode and the fast-wave limit: Analytic theory for tropical interannual oscillations and experiments in a hybrid coupled model. *J Atmos Sci* 48(4):584–606.
72. Jin F-F, Neelin JD (1993) Modes of interannual tropical ocean-atmosphere interaction —A unified view. Part I: Numerical results. *J Atmos Sci* 50(21):3477–3503.
73. Neelin JD, Jin F-F (1993) Modes of interannual tropical ocean-atmosphere interaction —A unified view. Part II: Analytical results in the weak coupling limit. *J Atmos Sci* 50(21):3504–3522.
74. Jin F-F, Neelin JD (1993) Modes of interannual tropical ocean-atmosphere interaction —A unified view. Part III: Analytical results in fully coupled cases. *J Atmos Sci* 50(21):3523–3540.
75. Jin F-F, Neelin JD, Ghil M (1994) El Niño on the devil’s staircase: Annual subharmonic steps to chaos. *Science* 264(5155):70–72.
76. Jin F-F, Neelin JD, Ghil M (1996) El Niño/Southern Oscillation and the annual cycle: Subharmonic frequency locking and aperiodicity. *Physica D* 98(2):442–465.
77. Kondrashov D, Sun C, Ghil M (2008) Data assimilation for a coupled ocean-atmosphere model. Part II: Parameter estimation. *Mon Weather Rev* 136(12):5062–5076.
78. Sun C, Hao Z, Ghil M, Neelin D (2002) Data assimilation for a coupled ocean-atmosphere model. Part I: Sequential state estimation. *Mon Weather Rev* 130(5):1073–1099.
79. Zebiak SE, Cane M (1987) A model of El Niño–Southern Oscillation. *Mon Weather Rev* 115(10):2262–2278.

